

Catalysis Science & Technology

Accepted Manuscript



This is an *Accepted Manuscript*, which has been through the Royal Society of Chemistry peer review process and has been accepted for publication.

Accepted Manuscripts are published online shortly after acceptance, before technical editing, formatting and proof reading. Using this free service, authors can make their results available to the community, in citable form, before we publish the edited article. We will replace this *Accepted Manuscript* with the edited and formatted *Advance Article* as soon as it is available.

You can find more information about *Accepted Manuscripts* in the [Information for Authors](#).

Please note that technical editing may introduce minor changes to the text and/or graphics, which may alter content. The journal's standard [Terms & Conditions](#) and the [Ethical guidelines](#) still apply. In no event shall the Royal Society of Chemistry be held responsible for any errors or omissions in this *Accepted Manuscript* or any consequences arising from the use of any information it contains.

Cite this: DOI: 10.1039/c0xx00000x

www.rsc.org/xxxxxx

ARTICLE TYPE

Light converting phosphors-based photocatalytic composites

Xinjuan Liu^{a,*}, Haipeng Chu^a, Jinliang Li^b, Lengyuan Niu^a, Can Li^a, Huili Li^b, Likun Pan^{b,*} and Chang Q. Sun^a

Received (in XXX, XXX) Xth XXXXXXXXX 20XX, Accepted Xth XXXXXXXXX 20XX

DOI: 10.1039/b000000x

Semiconductor photocatalysis has attracted tremendous attention due to its potential in environment remediation, clean energy production and chemical reaction technology. Pursuing high efficiency is a core task in the field. One of the major factors in photocatalysis is the limited light absorption of photocatalysts in the incident solar spectrum. In this treatise, we will survey the recent advancement of the light-conversion phosphors-based composites including up-conversion, down-conversion, and long afterglow phosphors-based composites for photocatalysis.

1 Introduction

Semiconductor photocatalysis as a green technology has attracted tremendous attention due to its great potential to solve environment and energy problems, since the research of photocatalytic water split on TiO₂ electrodes was conducted in 1972.¹⁻¹⁴ ZnO and TiO₂ semiconductors have been proven to be the promising photocatalysts for widespread environmental applications due to their intriguing optical and electric properties, low cost, and ease of availability.¹⁵⁻¹⁹ However, one of the major factors that limits their use is the mismatch between their band gap energy and the solar spectrum, which overlap only in the ultraviolet (UV) ($\lambda < 400$ nm) region. As a consequence, they can only utilize less than 5% of the solar energy impinging on the earth's surface, while visible light (~48%) and near infrared (NIR) light (~44%) cannot be effectively utilized.²⁰ Therefore, the exploration of efficient visible and NIR light photocatalysts has been an urgent issue from the viewpoint of utilization.²¹⁻²⁴

Currently, intensive investigations have been carried out to narrow the wide band gap of ZnO and TiO₂ to respond the visible light, including depositing with noble metal, doping with metal ions or non-metal elements and coupling with other narrow band gap semiconductors.²⁵⁻⁴² However, it is inevitably confronted with several disadvantages, such as poor stability, relatively low visible light absorption and increased carrier-recombination centres.⁴³⁻⁴⁸ Another attractive strategy is to design the novel visible light driven photocatalysts such as silver compounds (AgX (X = Cl, Br, I), Ag₂O, Ag₃PO₄, Ag₃VO₄, AgNbO₃, AgSbO₃),^{43,49,50} bismuth compounds (BiOX (X = Cl, Br, I), Bi₂MoO₆, BiVO₄, Bi₂WO₆),⁵¹⁻⁵⁶ indium complex oxides (InMO₄, M = V, Nb, Ta),⁵⁷ ternary chalcogenide compounds (AB_xC_y, A = Cu, Ag, Zn, Cd; B = Al, Ga, In; C = S, Se, Te, x, y = integer),⁵⁸ BaTaO₂N,⁵⁹ NaTaO₃,⁶⁰ et al. Traditional visible light driven photocatalysts such as Bi₂O₃ (55%),⁶¹ BiVO₄ (48%),⁶² Bi₂WO₆ (45%),⁶³ CdS (79%),⁷ MoS₂ (30%),⁶⁴ CuO (40%),⁶⁵ showed relatively low photocatalytic efficiency due to the

difficult separation of electron-hole pairs, which can still not be effectively applied for the solar cleaning up pollutant.⁶⁶⁻⁶⁹

The light-conversion phosphors (LCP) including up-conversion phosphors (UCP) and down-conversion phosphors (DCP), which transform lower (higher) energy phonons into higher (lower) energy photons, have attracted tremendous interest in recent years owing to their special electron structure and unique properties.⁷⁰⁻⁷³ Investigations have been carried out to study the LCP-semiconductor composites for photocatalysis.⁷²⁻⁷⁸ The LCP can absorb the given energy photon and emit other energy photon, which can be easily absorbed by given dye or effectively excite the semiconductor to generate more electron-hole pairs. Besides the light-converting ability, the long afterglow phosphors (LAP) as one kind of LCP can emit long lasting phosphorescence, which contributes to the persistent photocatalytic performance after turning off the irradiation light. Therefore, the incorporation of LCP into semiconductor to form hybrid materials has been proven to be a promising method to enhance the visible and NIR light photocatalysis, which should be a broad spectrum technology of environmental treatment.

In this work, the recent progress is highlighted in exploring various LCP-based composites for photocatalysis. Compared with traditional visible light driven photocatalysts, LCP/semiconductors composites exhibited enhanced photocatalytic activity. The mechanism of the improved photocatalytic activity under visible and NIR light irradiation is also discussed in detail. Although there are many reviews exploring UCP application in photocatalysis,²² there is distinct lack of reviews focusing specifically on DCP and LAP for photocatalysis.

2 Up-conversion phosphors

Extended utilization of sunlight from UV to visible or NIR light is an attractive issue in the field of photocatalysis.⁷⁹ The UCP can serve as a frequency conversion element for semiconductors to harvest light in a broader spectral range. Recently, the

incorporating UCP into semiconductors to form the hybrid materials has been reported to improve the photocatalytic activity of semiconductors.⁷⁵⁻⁷⁸ The possible photocatalytic mechanism in the presence of UCP/semiconductor hybrid photocatalysts was supposed as follows. The UCP doped in the semiconductor can absorb the NIR or visible lights and then emits UV or visible lights, as shown in Fig. 1, which can effectively excite the semiconductor to generate more electron-hole pairs and high active cavities, leading to the enhancement of photocatalytic activity of pure semiconductor.^{76,80-82} In the photocatalytic process, the holes on valence band not only directly decompose the organics adsorbed on the surface of semiconductor, but also oxidize water molecule to form $\cdot\text{OH}$ radicals with high activity and indirectly degrade the organics in aqueous solution.⁸³ In addition, the photo-generated electrons at conduction band could be accepted by the dissolved oxygen in water, triggering a successive one-electron reduction of O_2 to form $\text{O}_2^{\cdot-}$, HO_2^{\cdot} , H_2O_2 , and OH^{\cdot} . These radicals or reactive oxygen species are highly reactive with the organic pollutants, leading to the partial mineralization or complete mineralization of pollutants into CO_2 and H_2O . Beside the upconversion (UC) effect of UCP, the increased absorption, reduced electron-hole recombination, and enhanced oxygen vacancy signals are also beneficial to the photocatalytic activity of UCP/semiconductors hybrid materials compared to pure semiconductors.⁸³⁻⁸⁶ Therefore, the idea of UCP incorporation into the photocatalyst can be envisaged as an effective technology to treat wastewater using solar light irradiation.

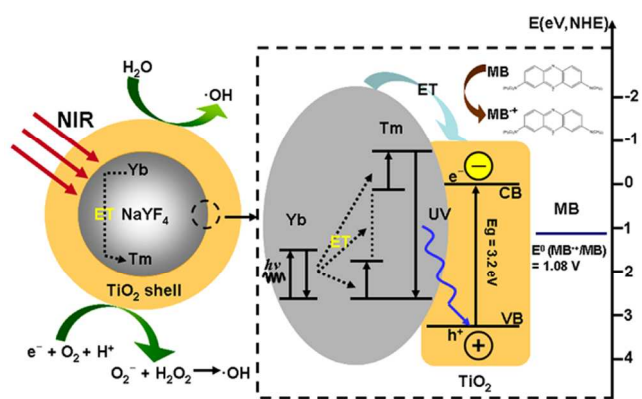


Fig. 1 Illustrative diagrams of energy transfer among UCP and TiO_2 ; and the generation of $\cdot\text{OH}$ radicals via the reaction of electron and hole with the surface species of TiO_2 . (Reprinted with permission from ref. ⁸⁰. Copyright (2013) American Chemical Society)

2.1 Oxide phosphors

Oxide phosphors such as $\text{Y}_3\text{Al}_5\text{O}_{12}:\text{Er}^{3+}$, $\text{YAlO}_3:\text{Er}^{3+}$, $\text{YFeO}_3:\text{Er}^{3+}$, and $\text{Y}_2\text{O}_3:\text{Yb}^{3+}, \text{Tm}^{3+}$ have been investigated due to their wide application in photocatalysis.⁸⁷ Attempts to combine the semiconductors such as TiO_2 , ZnO , Bi_2WO_6 , metal doped TiO_2 , and non-metal doped TiO_2 with the oxide phosphors have been made to form hybrid composites with superior photocatalytic activity.

2.1.1 $\text{Y}_3\text{Al}_5\text{O}_{12}:\text{Er}^{3+}$

$\text{Y}_3\text{Al}_5\text{O}_{12}:\text{Er}^{3+}$ can emit three UC fluorescent peaks in the range of 200-400 nm under the excitation of 488 nm, which can satisfy the

genuine requirement of TiO_2 , ZnO and Bi_2WO_6 photocatalysts.⁸⁸ Hence, $\text{Y}_3\text{Al}_5\text{O}_{12}:\text{Er}^{3+}$ -based composites can absorb efficiently the solar light in the photocatalytic process.

Pure Bi_2WO_6 presents the absorption from UV to visible light with wavelength of shorter than ca. 450 nm, as shown in Fig. 2, which occupies a small part of the solar spectrum.⁸⁵ Therefore, $\text{Y}_3\text{Al}_5\text{O}_{12}:\text{Er}^{3+}$ can convert visible light into UV light to excite Bi_2WO_6 effectively, leading to the enhancement of photocatalytic activity.⁸⁵ Moreover, $\text{Y}_3\text{Al}_5\text{O}_{12}:\text{Er}^{3+}/\text{Bi}_2\text{WO}_6$ photocatalysts show an increased absorption compared to pure Bi_2WO_6 . It had a high photocatalytic activity with a maximum degradation rate of 51% in the degradation of phenol (50 ml, 20 mg/l) than pure Bi_2WO_6 (31.5%) at 120 min under simulated solar light irradiation (500 W Xe lamp) due to the UC effect of $\text{Y}_3\text{Al}_5\text{O}_{12}:\text{Er}^{3+}$.

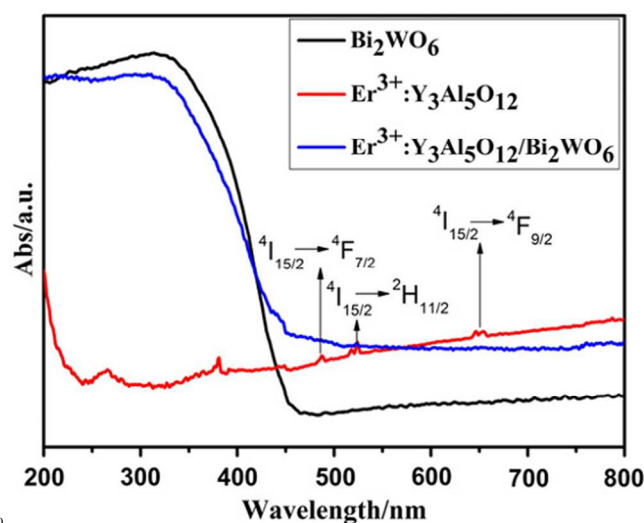


Fig. 2 UV-Vis diffuse reflectance spectra of the Bi_2WO_6 , $\text{Y}_3\text{Al}_5\text{O}_{12}:\text{Er}^{3+}$, $\text{Y}_3\text{Al}_5\text{O}_{12}:\text{Er}^{3+}/\text{Bi}_2\text{WO}_6$. (Reproduced with permission from ref. ⁸⁵)

Wang et al.^{73,89} found that photocatalytic activity of the $\text{Y}_3\text{Al}_5\text{O}_{12}:\text{Er}^{3+}/\text{anatase TiO}_2$ composites (1 g/l) prepared using sol-gel, ultrasonic dispersion and liquid boiling method was improved through the degradation of congo red (50 ml, 20 mg/l, rate constant of 0.4767 h^{-1}) and acid red B (50 ml, 10 mg/l, 89.95%) as compared with pure TiO_2 (0.0869 h^{-1} for congo red; 66.58% for acid red) under sunlight and visible light irradiation using triphosphor lamps with power of 144 W, correlated color temperature of 4000 K and intensity of 964347 lx. The similar experimental results were also reported in the literature.⁷⁷ However, the photocatalytic activity is still low due to the quick recombination of photo-induced electron-hole pairs. In order to further improve the photocatalytic activity of TiO_2 , the ZrO_2 was introduced into the $\text{TiO}_2/\text{Y}_3\text{Al}_5\text{O}_{12}:\text{Er}^{3+}$ composite by ultrasonic dispersion and liquid boiling method.⁷² The $\text{Y}_3\text{Al}_5\text{O}_{12}:\text{Er}^{3+}/\text{anatase TiO}_2/\text{ZrO}_2$ composite (1 g/l) had a high photocatalytic activity with a maximum degradation rate of 90.39% at 60 min in the degradation of Azo Fuchsine (100 ml, 10 mg/l) as compared with $\text{Y}_3\text{Al}_5\text{O}_{12}:\text{Er}^{3+}/\text{TiO}_2$ (77.99%), TiO_2 (27.86%) and $\text{Y}_3\text{Al}_5\text{O}_{12}:\text{Er}^{3+}/\text{ZrO}_2$ (5.74%) under solar light irradiation. When 7:3 Ti/Zr molar ratio, 500 °C and 50 min heat-treatment were adopted, the $\text{Y}_3\text{Al}_5\text{O}_{12}:\text{Er}^{3+}/\text{TiO}_2$ or ZrO_2 composite revealed the most efficient photocatalytic activity.⁷²

Recently, N and F co-doped $\text{Y}_3\text{Al}_5\text{O}_{12}:\text{Er}^{3+}$ was investigated

in order to change the crystalline field for broadening absorption range and enhancing emission spectra. The incorporation of N and F doped $Y_3Al_5O_{12}:Er^{3+}$ into TiO_2 to form hybrid materials may enlarge the visible light absorption range, and thus enhance the photocatalytic activity of TiO_2 . Yin et al.⁹⁰ synthesized successfully five types of photocatalysts, $Y_3Al_5O_{12}:Er^{3+}/TiO_2$, $Yb_nY_{3-n}Al_5O_{12}:Er^{3+}/TiO_2$, $Y_3Al_5N_xO_{12-x}:Er^{3+}/TiO_2$, $Y_3Al_5F_yO_{12-y}:Er^{3+}/TiO_2$ and $Yb_nY_{3-n}Al_5N_xF_yO_{12-x-y}:Er^{3+}/TiO_2$ by sol-gel method and investigated their photocatalytic activities in the degradation of acid red B dye (100 ml, 10 mg/l) under solar light irradiation. The TiO_2 in the composites shows the single anatase phase. The light irradiation intensity was $(2.0-2.5) \times 10^4 J/m^2$ min during April at 18-22 °C in Shenyang city (EL: 123.38° and NL: 41.80°) of China. It was suggested that the photocatalytic activity of TiO_2 can be enhanced largely by introducing the Yb, N and F doped $Y_3Al_5O_{12}:Er^{3+}$, and the $Yb_{0.3}Y_{2.7}Al_5N_{0.01}F_{0.01}O_{11.98}:Er^{3+}/TiO_2$ (1 g/l) displayed the highest photocatalytic activity with degradation rate of 91.74% at 60 min.

2.1.2 $YAlO_3:Er^{3+}$

$YAlO_3:Er^{3+}$ can emit the UV bands around 318.7 nm and 320.1 nm under the excitation of 486.5 nm and 542.4 nm, respectively.⁹¹ The UC luminescence around 326-342 nm and 354-359 nm was also detected under the excitation of red light around 652.2 nm (or 657.8 nm).⁹² Thus $YAlO_3:Er^{3+}$ can make full use of solar light and provide the rich UV light to excite the TiO_2 , ZnO or their composites, and thus enhance their photocatalytic activities.⁹³⁻⁹⁶ The $YAlO_3:Er^{3+}$ content, heat-treated temperature and heat treated time in the preparation of $YAlO_3:Er^{3+}/TiO_2$ or ZnO composite played key roles in the degradation of acid red B (100 ml, 10 mg/l) under solar light irradiation (China, Shenyang area, E123° 24' N41° 50', 19-25 °C temperature from March to April at midmorning of 9:30-10:30 a.m.).⁹⁷⁻⁹⁹ Wang et al.⁹⁸ synthesized the $YAlO_3:Er^{3+}/ZnO$ composites by ultrasonic dispersion and liquid boil method and subsequent heat-treatment at 500 °C for 60 min, and found that the sample with 6.0 wt% $YAlO_3:Er^{3+}$ (1 g/l) revealed higher photocatalytic activity (86%) than pure ZnO (69%) in the degradation of acid red B at 60 min under solar light irradiation.

Furthermore, spherical activated carbon (SAC) supported TiO_2 photocatalyst doped with $YAlO_3:Er^{3+}$ was prepared using ultrasonic dispersion and sol-gel method and the photocatalytic activity was evaluated in the degradation of methyl orange (MO) (50 ml, 1 g/l) under visible light irradiation from a 18 W-LED lamp ($\lambda > 400$ nm) with two strong peaks at 455 nm and 552.9 nm.¹⁰⁰ The SAC acted as pollutant concentrating photocatalyst support. A maximum MO degradation rate of 90.8% was obtained by using the $YAlO_3:Er^{3+}/anatase TiO_2/SAC$ composites (20 g/l) calcinated at 700 °C at 120 min.

2.1.3 $YFeO_3:Er^{3+}$

Similar to $YAlO_3:Er^{3+}/TiO_2/SAC$, $YFeO_3:Er^{3+}/TiO_2/SAC$ should also be a good visible light photocatalyst in the degradation of organic pollutants. The photocatalytic activity of $YFeO_3:Er^{3+}/TiO_2/SAC$ (20 mg/l) composites synthesized by a modified sol-gel method with ultrasonic dispersion was evaluated by degradation of MO (50 ml, 500 mg/l) under visible light irradiation using 18 W LED lamp with two strong peaks at 455 nm and 552.9 nm.⁷⁶ The XRD pattern of $YFeO_3:Er^{3+}/TiO_2$ calcinated at 700 °C indicated the dominance of anatase phase over rutile phase. The $YFeO_3:Er^{3+}/TiO_2/SAC$ calcinated at 700

°C, in which the TiO_2 predominantly existed in the form of anatase along with a small fraction of rutile, achieved a maximum degradation rate of 92% at 80 min.⁷⁶

2.2 Fluoride phosphors

In the recent years, fluoride phosphors have attracted much attention owing to their potential application in white LEDs, optical and photovoltaic devices.¹⁰¹ Similar to the oxide phosphors, fluoride phosphors such as $YF_3:Yb^{3+},Tm^{3+}$, $NaYF_4:Yb^{3+},Tm^{3+}$, $NaLuF_4:Gd^{3+},Yb^{3+},Tm^{3+}$ were also reported to extend the absorption of photocatalysts up to visible even to NIR light region, and thus enhance their photocatalytic activity.⁸¹

2.2.1 $YF_3:Yb^{3+},Tm^{3+}$

Under the excitation of a 980 nm laser, the emission peaks at 347 nm, 362 nm, 452 nm, and 476 nm were observed for $YF_3:Yb^{3+},Tm^{3+}$, which are assigned to $^1I_6 \rightarrow ^3F_4$, $^1D_2 \rightarrow ^3H_6$, $^1D_2 \rightarrow ^3F_4$, and $^1G_4 \rightarrow ^3H_6$ transitions, respectively.¹⁰² Therefore, it is appropriate candidate for NIR photocatalysis.

$YF_3:Yb^{3+},Tm^{3+}/TiO_2(P25)/graphene$ composites prepared via a one-step hydrothermal method exhibited great adsorptivity of dyes, significantly extended light absorption range, efficient charge separation properties and good stability due to the synergetic interactions among the components.¹⁰² The ternary composites (0.3 g/l) could effectively degrade the MO dye (100 ml, 0.02 g/l) under sunlight irradiation at 60 min with a higher degradation rate (78%) than the P25 (27%), $YF_3:Yb^{3+},Tm^{3+}/P25$ (46%) and P25/graphene (53%). In photocatalytic process, a 150 W high-pressure Xe lamp with illumination intensity of 100 mW/cm² was used to provide a full-spectrum emission with an AM 1.5 filter to simulate the sunlight source. Furthermore, the degradation rate of MO for P25 was 27%, which may be due to the presence of rutile phase of TiO_2 that can absorb some part of visible light up to 410 nm.

The core-shell structures are powerful platforms for the application in photocatalysis due to their excellent mechanical, optical, electrical and chemical properties.^{82,84,103-106} Qin et al.¹⁰⁷ synthesized the novel $YF_3:Yb^{3+},Tm^{3+}@anatase TiO_2$ core-shell nanoparticles by a modified hydrolysis method using polyvinylpyrrolidone K-30 as the coupling agent for photocatalysis. The average thickness of TiO_2 shells was about 10 nm, which is beneficial to the penetration of NIR light into the cores. The $YF_3:Yb^{3+},Tm^{3+}@TiO_2$ nanoparticles were able to efficiently degrade the methyl blue (MB) (500 ml, 15 mg/l) with a degradation rate of 58% at 9 h under the NIR light irradiation from sunlight (from 08:00 am-16:00 pm on 25-29 April 2009 in Changchun China with a cut off filter ($\lambda < 700$ nm)), which demonstrated that the NIR light could be used as the driving source for photocatalysis besides the UV and visible energy.¹⁰⁷

However, the shape of $YF_3:Yb^{3+},Tm^{3+}@TiO_2$ core-shell nanoparticles in above work was irregular with low quality, which might limit their photocatalytic activity. Development of uniform UCP- TiO_2 core-shell structures with desirable morphology will be advantageous for their photocatalytic applications. Ye et al.¹⁰⁸ prepared the uniform $YF_3:Yb^{3+},Tm^{3+}$ nanocrystals, which provided a good substrate to coat a anatase TiO_2 layer. As shown in Fig. 3(a) and (b), the $YF_3:Yb^{3+},Tm^{3+}$ nanocrystals with diameters of 50 ± 20 nm at ends and 25 ± 10 nm at centres are hierarchically organized together, showing an assembly structure with peanut-like geometry. The porous TiO_2

shells was coated on the $\text{YF}_3:\text{Yb}^{3+}, \text{Tm}^{3+}$ nanoparticles via sol-gel process and crystallized through annealing, as shown in Fig. 3(c) and (d). It is found that an obvious TiO_2 shell with thickness of 20 ± 10 nm is formed on surface of $\text{YF}_3:\text{Yb}^{3+}, \text{Tm}^{3+}$ particles. The $\text{YF}_3:\text{Yb}^{3+}, \text{Tm}^{3+}@\text{anatase TiO}_2$ (1 g/l) core-shell nanostructures not only possessed superior photocatalytic activity in the degradation of MO (20 ml, 50 mg/l) under the visible light irradiation (50 W Xe lamp) but also worked in the NIR light region, as the core $\text{YF}_3:\text{Yb}^{3+}, \text{Tm}^{3+}$ nanoparticles can efficiently up-convert NIR light into UV light.

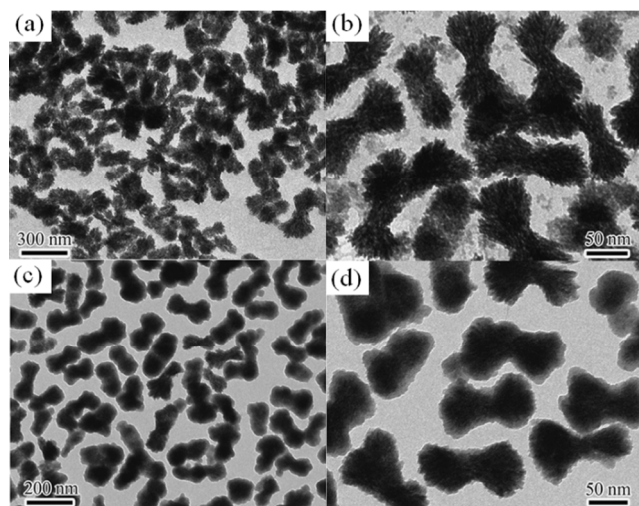


Fig. 3 Transmission electron microscopy (TEM) images of (a, b) $\text{YF}_3:\text{Yb}^{3+}, \text{Tm}^{3+}$ nanocrystals and (c, d) $\text{YF}_3:\text{Yb}^{3+}, \text{Tm}^{3+}@\text{TiO}_2$ particles. (Reproduced with permission from ref. ¹⁰⁸)

2.2.2 $\text{NaYF}_4:\text{Yb}^{3+}, \text{Tm}^{3+}/\text{Er}^{3+}$

Rare earth doped NaYF_4 has been widely studied in recent years. Quantum efficient in the range of 0.005% to 3% was obtained for the green emission of several NaYF_4 : 20% Yb^{3+} , 2% Er^{3+} nanoparticles with different particle sizes and a bulk sample.^{109,110}

Compared to YF_3 , rare earth doped NaYF_4 is a more effective UCP, which can emit bright light, such as green, blue, etc., under NIR light excitation.¹¹¹ The emitted bright fluorescence can be easily absorbed by semiconductors such as TiO_2 , ZnO and CdS to produce more electron-hole pairs, leading to the enhancement of their photocatalytic activity.¹¹²⁻¹¹⁶ Presently, one of the main problems for the new type of NIR-responsive photocatalysts is their low photocatalytic activity. How to improve the photocatalytic activity is a challenging issue.

Recently, researchers reported that the photocatalytic activity was obviously enhanced by using the $\text{NaYF}_4:\text{Yb}^{3+}, \text{Tm}^{3+}@\text{TiO}_2$ or ZnO core-shell nanocrystals compared to the pure TiO_2 or ZnO .^{82,117,118} These core-shell composites exhibited three emission peaks at 291 nm, 345 nm, and 361 nm, corresponding to the $^1\text{I}_6 \rightarrow ^3\text{H}_6$, $^1\text{I}_6 \rightarrow ^3\text{F}_4$, and $^1\text{D}_2 \rightarrow ^3\text{H}_6$ transitions of Tm^{3+} ions, respectively, which overlap with the absorption range of TiO_2 or ZnO .^{118,119} The core-shell structure may protect the UC core from surface quenching and increase the energy transfer efficiency. Therefore, these core-shell structures are effective photocatalysts for the degradation of organic pollutants under NIR light irradiation.

Fig. 4 shows typical TEM images of $\text{NaYF}_4:\text{Yb}^{3+}, \text{Tm}^{3+}$ nanocrystals and $\text{NaYF}_4:\text{Yb}^{3+}, \text{Tm}^{3+}@\text{TiO}_2$ nanoparticles.⁸⁰ The

TiO_2 shells are deposited around the $\text{NaYF}_4:\text{Yb}^{3+}, \text{Tm}^{3+}$ nanoparticles with the diameter of about 25 nm. When hydrothermally annealed at 160 °C, the TiO_2 shells are broken and lots of TiO_2 nanocrystals are dispersed around the $\text{NaYF}_4:\text{Yb}^{3+}, \text{Tm}^{3+}$ nanoparticles (Fig. 3(c)). TiO_2 nanocrystals show a d -spacing of 0.351 nm, well-matched to the spacing of (101) of anatase TiO_2 (Fig. 3(d)).

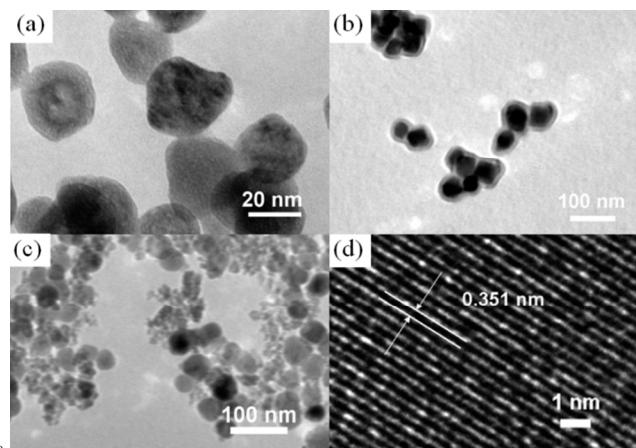


Fig. 4 TEM images of $\text{NaYF}_4:\text{Yb}^{3+}, \text{Tm}^{3+}$ nanocrystals (a), core-shell $\text{NaYF}_4:\text{Yb}^{3+}, \text{Tm}^{3+}@\text{TiO}_2$ nanoparticles (b) before and (c) after hydrothermal annealing, (d) high-resolution TEM of TiO_2 . (Reprinted with permission from ref. ⁸⁰. Copyright (2013) American Chemical Society)

Fig. 5 shows the photoluminescence (PL) spectra of $\text{NaYF}_4:\text{Yb}^{3+}, \text{Tm}^{3+}$, $\text{NaYF}_4:\text{Yb}^{3+}, \text{Tm}^{3+}@\text{anatase TiO}_2$ core-shell composite, and $\text{NaYF}_4:\text{Yb}^{3+}, \text{Tm}^{3+}-\text{TiO}_2$ physical mixture under 980 nm excitation.⁸⁰ Compared to pure $\text{NaYF}_4:\text{Yb}^{3+}, \text{Tm}^{3+}$, the emission peaks for $\text{NaYF}_4:\text{Yb}^{3+}, \text{Tm}^{3+}@\text{TiO}_2$ core-shell composite and physical mixture at 347 nm and 362 nm decrease significantly, while the peaks at 452 and 474 nm remain almost unchanged. But the emission peak for $\text{NaYF}_4:\text{Yb}^{3+}, \text{Tm}^{3+}@\text{anatase TiO}_2$ core-shell at 291 nm nearly disappears. The different energy migration processes affect markedly the photocatalytic activity of TiO_2 .

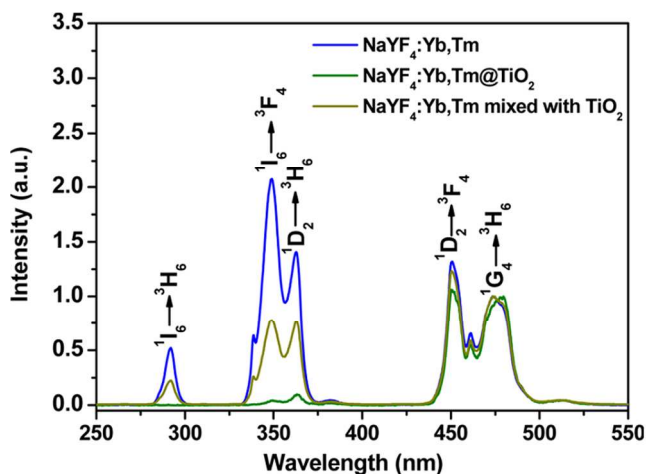


Fig. 5 PL spectra of $\text{NaYF}_4:\text{Yb}^{3+}, \text{Tm}^{3+}$, $\text{NaYF}_4:\text{Yb}^{3+}, \text{Tm}^{3+}@\text{TiO}_2$ core-shell composite, and $\text{NaYF}_4:\text{Yb}^{3+}, \text{Tm}^{3+}-\text{TiO}_2$ physical mixture under 980 nm excitation at room temperature. (Reprinted with permission from ref. ⁸⁰. Copyright (2013) American Chemical Society)

MB compound as a model pollutant (0.5 ml, 15 mg/l) was used to investigate the photocatalytic activity of $\text{NaYF}_4:\text{Yb}^{3+},\text{Tm}^{3+}$ @anatase TiO_2 composites (1 g/l) under NIR irradiation using a diode laser of 980 nm with a power of 10 W/cm^2 .⁸⁰ As shown in Fig. 6, the $\text{NaYF}_4:\text{Yb}^{3+},\text{Tm}^{3+}$ @anatase TiO_2 composite achieves a 65% degradation rate at 14 h, which is much higher than those of pure $\text{NaYF}_4:\text{Yb}^{3+},\text{Tm}^{3+}$ (8%) and $\text{NaYF}_4:\text{Yb}^{3+},\text{Tm}^{3+}$ - TiO_2 physical mixture (30%).⁸⁰ The energy transfer process between $\text{NaYF}_4:\text{Yb}^{3+},\text{Tm}^{3+}$ and TiO_2 is an important factor in the photocatalytic process.

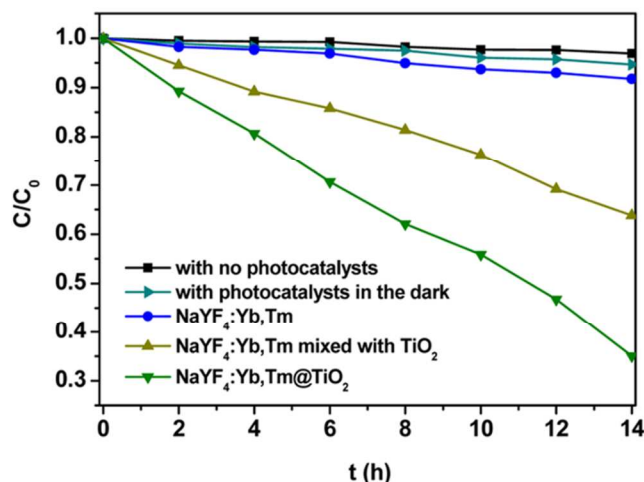


Fig. 6 Time-dependent ratios of C/C_0 in the presence of $\text{NaYF}_4:\text{Yb}^{3+},\text{Tm}^{3+}$, $\text{NaYF}_4:\text{Yb}^{3+},\text{Tm}^{3+}$ @ TiO_2 core-shell composite, and $\text{NaYF}_4:\text{Yb}^{3+},\text{Tm}^{3+}$ - TiO_2 physical mixture. (Reprinted with permission from ref.⁸⁰ Copyright (2013) American Chemical Society)

Zhang et al.¹¹⁹ further prepared the $\text{NaYF}_4:\text{Yb}^{3+},\text{Tm}^{3+}$ @anatase TiO_2 core-shell composites with different shell thickness by varying the ratio of fluoride rods and Ti precursors via a facile hydrothermal method, and studied their photocatalytic activities. The degradation rate for $\text{NaYF}_4:\text{Yb}^{3+},\text{Tm}^{3+}$ @anatase TiO_2 (0.04 M TiF_4 , 10 g/l) reached a maximum value of 90% for MB (1 ml, 5 mg/l) at 12 h under NIR irradiation using a 1.5 W 980 nm diode laser.¹¹⁹ Similarly, the incorporation of $\text{NaYF}_4:\text{Yb}^{3+},\text{Tm}^{3+}$ into ZnO composites was also shown to greatly promote the photocatalytic activity in the degradation of RhB (0.5 ml, 20 mg/l) with a degradation rate of 65% at 30 h under NIR irradiation using a diode laser of 980 nm with a power density of 2.0 W/cm^2 , whereas $\text{NaYF}_4:\text{Yb}^{3+}$, $\text{NaYF}_4:\text{Yb}^{3+},\text{Tm}^{3+}$ and ZnO aqueous suspensions showed very limited photocatalytic activity.¹¹⁸

Wang et al.¹²⁰ successfully synthesized the double-shell-structured $\text{NaYF}_4:\text{Yb}^{3+},\text{Tm}^{3+}$ or Er^{3+} @ SiO_2 @ TiO_2 photocatalysts by a simple hydrothermal method, and studied the influence of different UCP in affecting the NIR-driven photocatalysis. They consist of uniform $\text{NaYF}_4:\text{Yb}^{3+},\text{Tm}^{3+}$ or Er^{3+} nanocrystals, SiO_2 as the media shell, and anatase TiO_2 nanocrystals exposed with the high-reactive facets as the outer shell, as shown in Fig. 7(a)-(c). The thickness of SiO_2 shell is about 30 nm (Fig. 7(g)). The outer TiO_2 shell is composed of a large amount of nanocrystals with the diameter of about 20 nm (Fig. 7(h,i)). The photocatalytic activity of the photocatalysts (1 g/l) was evaluated by the degradation of RhB (10^{-5} M) under the NIR irradiation (3 W/mm^2), and the photocatalytic activity of $\text{NaYF}_4:\text{Yb}^{3+},\text{Tm}^{3+}$ @ SiO_2 @ TiO_2 was

found to be higher (0.3624 h^{-1}) than that of $\text{NaYF}_4:\text{Yb}^{3+},\text{Er}^{3+}$ @ SiO_2 @ TiO_2 (0.2912 h^{-1}).

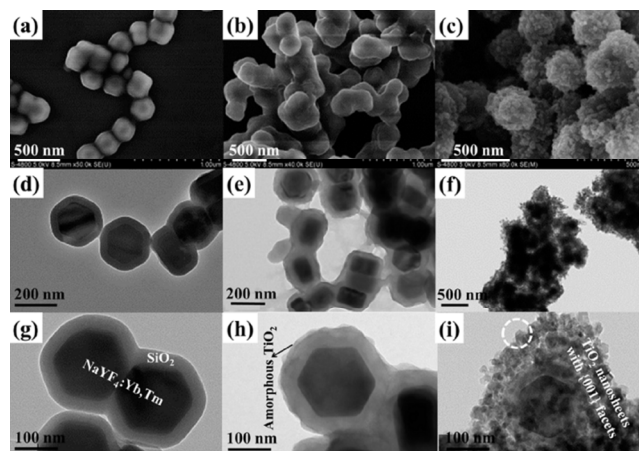


Fig. 7 Scanning electron microscopy (SEM) and TEM images of (a, d, g) $\text{NaYF}_4:\text{Yb}^{3+},\text{Tm}^{3+}$ @ SiO_2 , (b, e, h) $\text{NaYF}_4:\text{Yb}^{3+},\text{Tm}^{3+}$ @ SiO_2 @amorphous TiO_2 , and (c, f, i) $\text{NaYF}_4:\text{Yb}^{3+},\text{Tm}^{3+}$ @ SiO_2 @ TiO_2 . (Reprinted with permission from ref.¹²⁰ Copyright (2014) American Chemical Society)

2.2.3 $\text{CaF}_2:\text{Er}^{3+},\text{Tm}^{3+},\text{Yb}^{3+}$

$\text{Tm}^{3+},\text{Er}^{3+},\text{Yb}^{3+}$ co-doped CaF_2 nanoparticles with unique UC properties have been intensively studied.¹²¹ The UV (361 nm and 379 nm), violet (408 nm), and blue (485 nm) light from $\text{Tm}^{3+},\text{Er}^{3+},\text{Yb}^{3+}$ co-doped CaF_2 nanoparticles can be harvested by semiconductors for photocatalysis.^{83,84} Huang et al.⁸³ prepared a novel $\text{CaF}_2:\text{Er}^{3+},\text{Tm}^{3+},\text{Yb}^{3+}/\text{BiVO}_4$ photocatalyst with dendritic structure via a two-step hydrothermal method. The $\text{CaF}_2:\text{Er}^{3+},\text{Tm}^{3+},\text{Yb}^{3+}$ particles with an average particle size of 140 nm were dispersed homogeneously on the dendritic surface of BiVO_4 . The absorption and emission intensities of the $\text{CaF}_2:\text{Er}^{3+},\text{Tm}^{3+},\text{Yb}^{3+}/\text{BiVO}_4$ composite were higher than those of pure $\text{CaF}_2:\text{Er}^{3+},\text{Tm}^{3+},\text{Yb}^{3+}$ or BiVO_4 , through tailoring the crystal symmetry of lanthanide ions by Bi^{3+} ions. The degradation rate of MO (10 ml, 10 mg/l) for $\text{CaF}_2:\text{Er}^{3+},\text{Tm}^{3+},\text{Yb}^{3+}/\text{BiVO}_4$ (2 g/l) was improved ($0.113 \times 10^{-1} \text{ h}^{-1}$) under 980 nm NIR irradiation compared to the pure $\text{CaF}_2:\text{Er}^{3+},\text{Tm}^{3+},\text{Yb}^{3+}$ or BiVO_4 .⁸³ Furthermore, the same group also found that the $\text{CaF}_2,\text{Tm}^{3+},\text{Yb}^{3+}$ @anatase TiO_2 photocatalyst had higher photocatalytic activity in the degradation of MB ($4.96 \times 10^{-2} \text{ mg}/\text{lh}$) and MO ($2.67 \times 10^{-2} \text{ mg}/\text{lh}$) than pure TiO_2 , $\text{Yb}^{3+},\text{Er}^{3+}$ co-doped TiO_2 and CaF_2 @ TiO_2 under NIR light irradiation.⁸⁶

CaWO_4 is a good oxide host material for lanthanide ions with high UC efficiency. The formation of lanthanide ions doped CaWO_4 or CaF_2 can fulfil the requirements of high stability and excellent UC properties. Huang et al.⁸⁴ synthesized a $\text{CaWO}_4:\text{Er}^{3+},\text{Tm}^{3+},\text{Yb}^{3+}$ @(anatase $\text{TiO}_2/\text{CaF}_2$) (ETY/CTC) photocatalyst via a hydrothermal method, and its photocatalytic activity (1 g/l) was tested through the degradation of MO (20 mg/l, 20 ml) under NIR light irradiation ($\lambda \cong 780 \text{ nm}$). ETY/CTC possessed higher photocatalytic activity compared to $\text{Er}^{3+},\text{Tm}^{3+},\text{Yb}^{3+}$ tri-doped CaWO_4 @ TiO_2 , owing to the enhanced UC property, the increased electron-hole separation efficiency and oxygen vacancy signals.⁸⁴

2.2.4 Other fluoride phosphors

Liu et al.¹²² investigated the influence of $10\text{BaF}_2:\text{NaF}$, Na_3AlF_6 doping on the visible light photocatalytic activity of TiO_2 with

anatase and rutile phase. $10\text{BaF}_2:\text{NaF},\text{Na}_3\text{AlF}_6$ displays two emission peaks at 304 nm and 324 nm under the excitation of 583 nm, and TiO_2 exhibits a narrow absorption band from 200 nm to 400 nm. The absorption band of TiO_2 overlaps very well with the UV emission of $10\text{BaF}_2:\text{NaF},\text{Na}_3\text{AlF}_6$. In the photocatalytic reduction of CO_2 with H_2O (400 ml) under visible light irradiation by a 500 W spherical Xe lamp with an optical filter ($\lambda > 515$ nm), $10\text{BaF}_2:\text{NaF},\text{Na}_3\text{AlF}_6/\text{TiO}_2$ (5 g/l) exhibited excellent photocatalytic activity (179 $\mu\text{mol/g-cat}$) under visible light irradiation.¹²²

Silimar to $10\text{BaF}_2:\text{NaF},\text{Na}_3\text{AlF}_6$, the $40\text{CdF}_2\cdot 60\text{BaF}_2\cdot 1.0\text{Er}_2\text{O}_3$ can emit five UC fluorescent peaks under the excitation of 488 nm, and supply the UV light for the TiO_2 photocatalyst. By calculation, the UC efficiency of the emission peak at 380 nm was estimated to be about 0.78%. Wang et al.¹²³⁻¹²⁵ prepared the $40\text{CdF}_2\cdot 60\text{BaF}_2\cdot 1.0\text{Er}_2\text{O}_3/\text{rutile TiO}_2$ photocatalyst by ultrasonic and boiling dispersion at 80 kHz frequency with 50 W output power for 15 min and studied its photocatalytic activity through the degradation of azo fuchsine, ethyl violet and acid red B (10 mg/l) solution under visible light irradiation using triphosphor lamps with color temperature of 4000 K and light intensity of 964347 lx). $40\text{CdF}_2\cdot 60\text{BaF}_2\cdot 1.0\text{Er}_2\text{O}_3/\text{rutile TiO}_2$ powder (1 g/l) showed a higher photocatalytic activity in the degradation of azo fuchsine (95%), ethyl violet (87%), and acid red B (100%) than undoped TiO_2 .

3 Down-conversion phosphors

Great efforts indicated that photocatalytic degradation of dyes in wide band gap semiconductor suspension under visible light irradiation is a typical self-sensitized degradation process.¹²⁶⁻¹³² In the photocatalytic process, the dye is excited under visible light irradiation to dye*. The photo-induced electrons are transferred from dye* to semiconductors and then react with adsorbed oxidants, usually O_2 , to produce reactive oxygen radicals (O_2^-).^{4,132-134} However, the photocatalytic degradation rate and mineralization degree of dyes are limited because of the slow interfacial electron transfer.⁵² The DCP has attracted tremendous attention in recent years due to their intrinsic and unique conversion properties.^{70,72,73,135-137} Recently, many studies indicated that the incorporation of the DCP into photocatalyst to form hybrid materials can enhance the visible light photocatalytic activity of the wide band gap semiconductor by utilizing the light down-converting characteristics of the phosphors to facilitate the self-degradation of MB. The possible photocatalytic mechanism in the presence of DCP/semiconductor hybrid photocatalysts was supposed as follows. The DCP can absorb the high energy photon and emit the low energy photon at a longer wavelength, which can be easily absorbed by given dye and thus effectively excite the dye to generate more electron-hole pairs, resulting in the improvement of the self-sensitized degradation of dye.^{74,126,138} Moreover, the increase of dye adsorption and visible light absorption as well as the reduction of electron-hole pair recombination in wide band gap semiconductor should also be responsible for the enhancement of the photocatalytic performance.^{74,126,138} Therefore, the incorporation of the DCP into photocatalyst to form hybrid materials should be a promising method to enhance the visible light photocatalysis.

3.1 Oxide phosphors

The light converting ability of oxide phosphors is promising to fulfil a simple and effective removal of dyes by adjusting the light emission of the oxide phosphors to improve the self-sensitized degradation of dyes. Therefore, exploration of oxide phosphor-semiconductor composites and study the effect of their down-converting (DC) property on the self-sensitized degradation of different dyes is necessary for better understanding of this technique and the mechanism behind.

3.1.1 $\text{Y}_3\text{Al}_5\text{O}_{12}:\text{Ce}^{3+}$

$\text{Y}_3\text{Al}_5\text{O}_{12}:\text{Ce}^{3+}$ shows two absorption peaks at 340 nm and 455 nm, which are assigned to the characteristic $4f^1 \rightarrow 5d^1$ transition of Ce^{3+} ions. A broad emission spectrum with a peak at 525 nm for $\text{Y}_3\text{Al}_5\text{O}_{12}:\text{Ce}^{3+}$ under the excitation of 455 nm falls in the absorption range of the dye MB (< 663 nm) well, which indicates that $\text{Y}_3\text{Al}_5\text{O}_{12}:\text{Ce}^{3+}$ can be used as effective DCP to improve the self-sensitized degradation of the dye MB.

Jiang et al.¹³⁹ indicated that $\text{Y}_3\text{Al}_5\text{O}_{12}:\text{Ce}^{3+}/\text{anatase TiO}_2$ compound films exhibited a superior photocatalytic activity in the degradation of MB (50 ml, 12 mg/l) under UV light irradiation using 160 W high pressure mercury lamp than the pure TiO_2 film due to its larger specific surface area, stronger absorption and higher photo-generated current density with the introduction of $\text{Y}_3\text{Al}_5\text{O}_{12}:\text{Ce}^{3+}$. Unfortunately, the DC property of $\text{Y}_3\text{Al}_5\text{O}_{12}:\text{Ce}^{3+}$ had not been utilized in above the work.

Pan et al.¹³⁸ reported that the introduction of $\text{Y}_3\text{Al}_5\text{O}_{12}:\text{Ce}^{3+}$ by utilizing the DC characteristics can facilitate the self-sensitized degradation of MB, thus enhance the photocatalytic activity of ZnO. $\text{ZnO}/\text{Y}_3\text{Al}_5\text{O}_{12}:\text{Ce}^{3+}$ composites were successfully synthesized via microwave-assisted reaction of ZnO precursor with $\text{Y}_3\text{Al}_5\text{O}_{12}:\text{Ce}^{3+}$ suspension using a microwave synthesis system. As shown in Fig. 8, ZnO displays the sheet nanostructure and the $\text{Y}_3\text{Al}_5\text{O}_{12}:\text{Ce}^{3+}$ particles are monodisperse with diameters in the range of 200-300 nm. The photocatalytic activity of the $\text{ZnO}/\text{Y}_3\text{Al}_5\text{O}_{12}:\text{Ce}^{3+}$ composites (2 g/l) with 3 wt.% of $\text{Y}_3\text{Al}_5\text{O}_{12}:\text{Ce}^{3+}$ in the degradation of MB (5 mg/l) under visible light irradiation (400 W metal halogen lamp with wavelength: 390 nm-800 nm) was found to be much improved (93%) compared with pure ZnO (13%) mainly due to the DC effect of $\text{Y}_3\text{Al}_5\text{O}_{12}:\text{Ce}^{3+}$, which facilitated the self-sensitized destruction of MB.¹³⁸

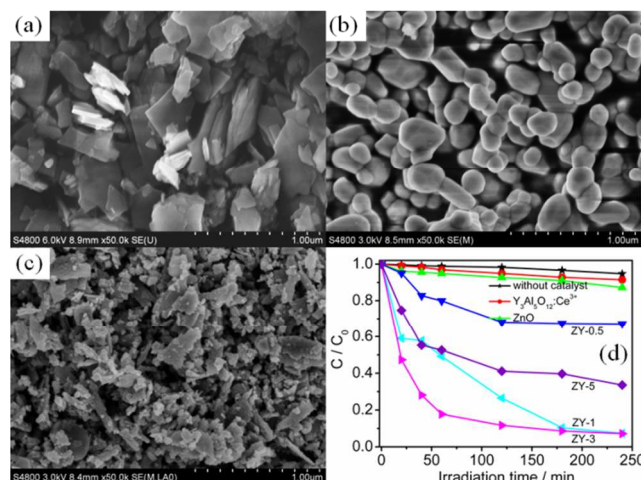


Fig. 8 FESEM images of (a) ZnO nanosheets, (b) $Y_3Al_5O_{12}:Ce^{3+}$ particles and (c) ZnO/ $Y_3Al_5O_{12}:Ce^{3+}$ composites with 3 wt.% $Y_3Al_5O_{12}:Ce^{3+}$; (d) photocatalytic degradation of MB by ZnO/ $Y_3Al_5O_{12}:Ce^{3+}$ composites with 0.5 (ZY-0.5), 1 (ZY-1), 3 (ZY-3) and 5 (ZY-5) wt.% $Y_3Al_5O_{12}:Ce^{3+}$. (Reproduced with permission from ref. ¹³⁸)

3.1.2 $Y_2O_3:Eu^{3+}$

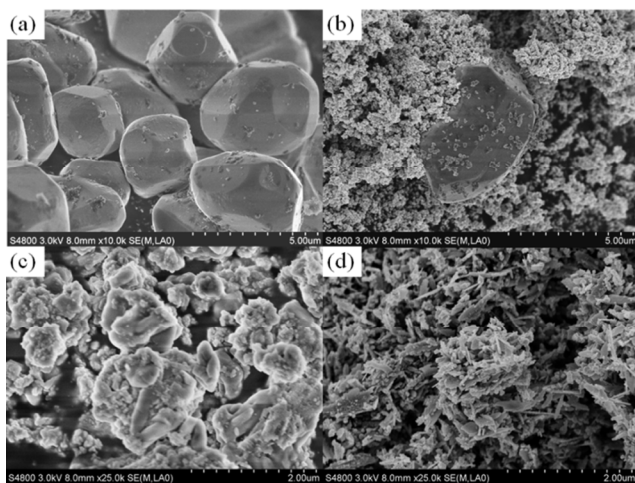


Fig. 9 FESEM images of (a) $Y_2O_3:Eu^{3+}$ and (b) ZnO/ $Y_2O_3:Eu^{3+}$ composites with 0.5 wt.% $Y_2O_3:Eu^{3+}$; (Reprinted with permission from ref. ¹²⁶. Copyright (2013) American Chemical Society) (c) $NaSrBO_3:Tb^{3+}$ and (d) ZnO/ $NaSrBO_3:Tb^{3+}$ composite with 1 wt.% $NaSrBO_3:Tb^{3+}$. (Reproduced with permission from ref. ⁷⁴)

Further study showed that such a light converting phenomenon was also found for ZnO/ $Y_2O_3:Eu^{3+}$ composites (2 g/l) synthesized microwave-assisted method for photocatalytic degradation of MB, RhB and MO (80 ml, 5 mg/l). $Y_2O_3:Eu^{3+}$ particles are monodisperse with diameters in the range of 3-5 μm , as shown in Fig. 9(a). The $Y_2O_3:Eu^{3+}$ is surrounded by the ZnO particles in the composite, as shown in the Fig. 9(b). The photocatalytic experimental results showed that $Y_2O_3:Eu^{3+}$ phosphors played an important role in the enhancement of visible light photocatalysis. ZnO/ $Y_2O_3:Eu^{3+}$ composites with 0.5 wt.% $Y_2O_3:Eu^{3+}$ exhibited the highest visible light photocatalytic activity in the degradation of MB (95%).

3.1.3 $NaSrBO_3:Tb^{3+}$

Pan et al.⁷⁴ further studied the ZnO/ $NaSrBO_3:Tb^{3+}$ composite synthesized via a microwave-assisted method for visible light photocatalytic degradation of MB, RhB, MO and reduction of Cr(VI) (80 ml, 5 mg/l). $NaSrBO_3:Tb^{3+}$ has a diameter in the range of 0.5-1 μm , as shown in Fig. 9(c). As shown in Fig. 10, the emission band of $NaSrBO_3:Tb^{3+}$ phosphors (about 540-700 nm) matches the absorption range of the MB (about 550-700 nm) and RhB (500-600 nm), but it cannot be absorbed by the MO (about 400-530 nm) and Cr(VI). Therefore, the emitted low energy photons by $NaSrBO_3:Tb^{3+}$ can be easily absorbed by the MB and RhB, and thus generate more electron-hole pairs, leading to the obvious improvement of the self-sensitized destruction of MB and RhB. However, it is not obviously enhanced in the degradation of MO or does not happen in the reduction of Cr(VI). The photocatalytic experimental results indicated that the maximum MB and RhB degradation rates for ZnO/ $NaSrBO_3:Tb^{3+}$ composite with 1 wt.% $NaSrBO_3:Tb^{3+}$ reached to 97% and 94%, respectively, while the degradation rates of MO and reduction rate of Cr(VI) were only 38% and 37%, respectively. The large

difference in the photocatalytic process indicates that the contribution of the light DC effect of $NaSrBO_3:Tb^{3+}$ to the photocatalytic performance by enhancing the self-sensitized degradation. Besides the self-sensitized degradation of dyes, the improvement of photocatalytic performance should also be ascribed to the increase of the visible light absorption and the reduction of electron-hole pair recombination in ZnO with the incorporation of $NaSrBO_3:Tb^{3+}$ (Fig. 11).

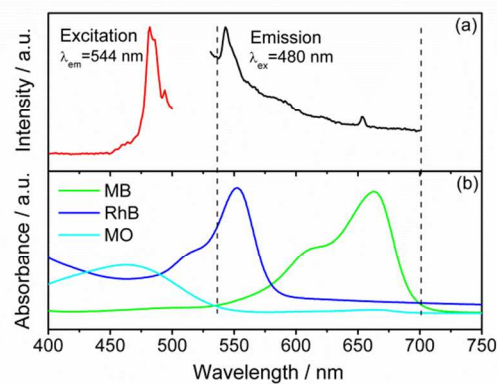


Fig. 10(a) PL excitation and emission spectra of $NaSrBO_3:Tb^{3+}$; (b) UV-vis absorption spectra of MB, RhB and MO. (Reproduced with permission from ref. ⁷⁴)

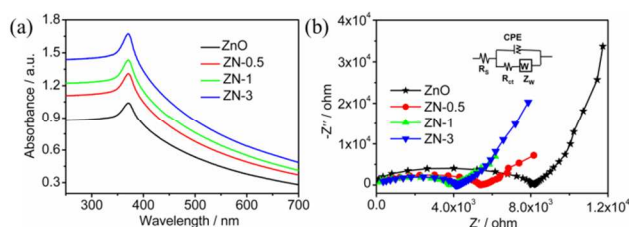


Fig. 11(a) UV-vis absorption spectra and (b) Nyquist plots of ZnO, ZN-0.5, ZN-1 and ZN-3. Inset is the corresponding equivalent circuit model. The ZnO/ $NaSrBO_3:Tb^{3+}$ composite with 0.5, 1, and 3 wt.% $NaSrBO_3:Tb^{3+}$ is named as ZN-0.5, ZN-1 and ZN-3. (Reproduced with permission from ref. ⁷⁴)

Besides the above mentioned oxide phosphors-based composites, $Gd_2O_3:Tb^{3+}$ or Sr_2CeO_4/TiO_2 composites also exhibited significantly improved photocatalytic activity over pure TiO_2 (P25) in degradation of gaseous benzene, MB (1×10^{-5} mol/l), and formaldehyde diluted in water (0.1 mol/l) under UV light irradiation (10 W, UV-A, 9 W/m²), which was ascribed to the synergy of electron transfer and the stronger absorption in the region 400-850 nm.^{140,141}

3.2 Other oxide phosphors

Recently, many oxide phosphors such as $SrWO_4:Ln^{3+}$ (Eu^{3+} , Tb^{3+} , Sm^{3+} and Dy^{3+}) and $Zn_3V_2O_8$ have been reported for photocatalytic degradation of dyes under visible light irradiation.¹⁴²

3.2.1 $SrWO_4:Ln^{3+}$ (Eu^{3+} , Tb^{3+} , Sm^{3+} and Dy^{3+})

Zheng et al.¹⁴² successfully prepared $SrWO_4:Ln^{3+}$ (Eu^{3+} , Tb^{3+} , Sm^{3+} and Dy^{3+}) phosphors by the microwave treatment at very low temperature (70 °C) for only 45 min. Upon excitation at 248 nm, the green emission peaks at 490, 545, 583 and 622 nm for $SrWO_4:Ln^{3+}$ could be observed, which were transitions from the

5D_4 excited state to the different J levels of the ground state 7F_J ($J = 6, 5, 4, 3$). The photocatalytic activity of $\text{SrWO}_4:\text{Ln}^{3+}$ (Eu^{3+} , Tb^{3+} , Sm^{3+} and Dy^{3+}) was examined by the degradation of different dyes (MB, MO and RhB) under mercury lamp irradiation (a 500 W mercury lamp with a maximum emission at 365 nm). An obvious reduction in the absorption peaks for all three dyes was observed in the presence of $\text{SrWO}_4:\text{Tb}^{3+}$, $\text{SrWO}_4:\text{Dy}^{3+}$ and $\text{SrWO}_4:\text{Sm}^{3+}$ after UV light illumination at 70 min. In addition, MB was decomposed dramatically during the irradiation period using $\text{SrWO}_4:\text{Eu}^{3+}$ phosphors, but the MO and RhB were hardly degraded, which is because that the emission of $\text{SrWO}_4:\text{Eu}^{3+}$ located in the red region (600-700 nm) only overlaps with the absorption of MB.¹⁴²

3.2.2 $\text{Zn}_3\text{V}_2\text{O}_8$

Recently, vanadate has attracted much attention because of its rich structural chemistry and wide applications in photocatalyst and optoelectronic device. $\text{Zn}_3\text{V}_2\text{O}_8$ as a typical vanadate has an interesting crystal structure that is of porous framework. $\text{Zn}_3\text{V}_2\text{O}_8$, with broadband yellowish white emission, was synthesized via combustion route, hydrothermal, sol-gel, and solid state reaction methods.¹⁴³ $\text{Zn}_3\text{V}_2\text{O}_8$ prepared by the combustion method showed the spherical particles with dimension between 1 and 3 μm . The hydrothermally treated $\text{Zn}_3\text{V}_2\text{O}_8$ at 150 °C for 24 h and sintered at 775 °C for 12 h showed thin plate like particles with the average size of 3-5 μm , which connected with each other and formed flower like structure. $\text{Zn}_3\text{V}_2\text{O}_8$ prepared by sol-gel method displayed the cylindrical particles with diameters of 10-12 μm long and 2-3 μm diameters. Much bigger and rough microstructure of $\text{Zn}_3\text{V}_2\text{O}_8$ was formed by the solid state reaction method. The photocatalytic activity of $\text{Zn}_3\text{V}_2\text{O}_8$ phosphors (250 mg/l) was investigated by the degradation of MB (400 ml, 10 mg/l) under visible light irradiation using 60 W halogen-tungsten lamp. It was found that the MB degradation rate for $\text{Zn}_3\text{V}_2\text{O}_8$ synthesized via hydrothermal method was highest compared to the other methods, which might be ascribed to its large surface area.¹⁴³

4 Long afterglow phosphors

Alkaline-earth aluminate phosphors have attracted considerable attention for their potential applications in the fields such as luminous paints, safety indicators and plasma display phosphors. Recently, many reports confirmed that coupling semiconductor with LAP such as blue $\text{CaAl}_2\text{O}_4:\text{Eu}^{2+}, \text{Nd}^{3+}$, green $\text{SrAl}_2\text{O}_4:\text{Eu}^{2+}, \text{Dy}^{3+}$ and $\text{BaAl}_2\text{O}_4:\text{Eu}^{2+}, \text{Dy}^{3+}$, can maintain the photocatalytic activity even after turning off the light for a long time. This is because that the LAP stores light from the light source and emits slowly, which excites the semiconductor to generate the more electron-hole pairs when the irradiation source is cut off.¹⁴⁴ Such a self-fluorescence-assisted system could enhance the photocatalytic activity for environmental clean-up.¹⁴⁵ It is a new concept for the photocatalyst synthesis and applications.

4.1 Aluminates phosphors

4.1.1 $\text{CaAl}_2\text{O}_4:\text{Eu}^{2+}, \text{Nd}^{3+}$

$\text{CaAl}_2\text{O}_4:\text{Eu}^{2+}, \text{Nd}^{3+}$ is an excellent LAP due to its good chemical stability, low toxicity, and long afterglow time.¹⁰³ The photocatalytic activity of $\text{CaAl}_2\text{O}_4:\text{Eu}^{2+}, \text{Nd}^{3+}$ -based

composites has been reported in the degradation of dye pollutants.

Yoon et al.^{146,147} prepared the $\text{CaAl}_2\text{O}_4:\text{Eu}^{2+}, \text{Nd}^{3+}/\text{anatase TiO}_2$, and $\text{CaAl}_2\text{O}_4:\text{Eu}^{2+}, \text{Nd}^{3+}/\text{anatase TiO}_2/\text{Al}_2\text{O}_3$ composites using a sol-gel processing and atomic layer deposition method and their photocatalytic activity was evaluated by the degradation of MB (1.6×10^{-5} mol/ml, 100 ml) aqueous solution under visible light irradiation using a 100 W white light lamp with a cutoff filter ($\lambda > 400$ nm). The composites showed much higher photocatalytic activity than pure TiO_2 , which might be because the combination of TiO_2 with phosphors induced energy band bending at the junction, shifted the absorption band of the TiO_2 toward the visible light region, and thus increased the electron-hole pairs. However, no noticeable degradation was observed after turning off the light.

$\text{TiO}_{2-x}\text{N}_y$ showed visible light absorption up to 700 nm, which had a perfect overlap with the emission spectrum of $\text{CaAl}_2\text{O}_4:\text{Eu}^{2+}, \text{Nd}^{3+}$, as shown in Fig. 12.¹⁴⁸ Therefore, the $\text{CaAl}_2\text{O}_4:\text{Eu}^{2+}, \text{Nd}^{3+}$ -based hybrid materials could use the long afterglow from the phosphor as the light source in the photocatalytic reaction process. Li et al.¹⁴⁹⁻¹⁵² prepared the $\text{CaAl}_2\text{O}_4:\text{Eu}^{2+}, \text{Nd}^{3+}/\text{brookite TiO}_{2-x}\text{N}_y$ composites in a sequence of procedures, which involved reactions of TiCl_3 and hexamethylenetetramine mixed solution at 190 °C for 2 h to obtain the brookite $\text{TiO}_{2-x}\text{N}_y$, followed by mixing with $\text{CaAl}_2\text{O}_4:\text{Eu}^{2+}, \text{Nd}^{3+}$ particles by a soft planetary ball milling. $\text{CaAl}_2\text{O}_4:\text{Eu}^{2+}, \text{Nd}^{3+}/\text{brookite TiO}_{2-x}\text{N}_y$ showed higher persistent NO destruction ability in dark after turning off the exciting light compared to pure $\text{TiO}_{2-x}\text{N}_y$.¹⁵¹ With the increase in $\text{TiO}_{2-x}\text{N}_y$ content to 40 wt.%, the photocatalytic activity increased. However with further increase in $\text{TiO}_{2-x}\text{N}_y$ content, the photocatalytic activity slight decreased, which might be due to the decrease in the fluorescence intensity of $\text{CaAl}_2\text{O}_4:\text{Eu}^{2+}, \text{Nd}^{3+}$.^{149,152}

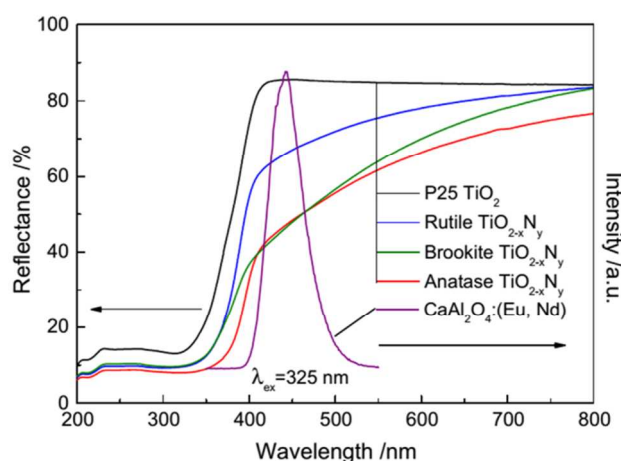


Fig. 12 Overlap of the diffuse reflectance spectra and emission spectra of uncoupled $\text{CaAl}_2\text{O}_4:\text{Eu}^{2+}, \text{Nd}^{3+}$ and $\text{CaAl}_2\text{O}_4:\text{Eu}^{2+}, \text{Nd}^{3+}/\text{TiO}_{2-x}\text{N}_y$ composite. (Reproduced with permission from ref. ¹⁴⁸)

Li et al.^{153,154} synthesized the $\text{SrTi}_{1-x}\text{Cr}_y\text{O}_3$ nanoparticles with a diameter of 25-40 nm to couple with $\text{CaAl}_2\text{O}_4:\text{Eu}^{2+}, \text{Nd}^{3+}$ though a simple precipitation method. The $\text{CaAl}_2\text{O}_4:\text{Eu}^{2+}, \text{Nd}^{3+}/\text{SrTi}_{1-x}\text{Cr}_y\text{O}_3$ composites exhibited prolonged photocatalytic activity in the oxidative destruction of NO in a continuous gas

flow system even after turning off light at 180 min. The photocatalytic activity was dependent on the proportion of $\text{SrTi}_{1-x}\text{Cr}_x\text{O}_3$ in the composites and the optimal content was around 50 wt.%.¹⁵³ Similarly, the $\text{CaAl}_2\text{O}_4:\text{Eu}^{2+},\text{Nd}^{3+}/\text{SrTiO}_3/\text{Fe}_2\text{O}_3$ composites synthesized using the microwave-assisted solvothermal method could also efficiently degrade the NO gas not only under UV light irradiation using a 450 W high pressure mercury lamp but also in the dark with fluorescence assistance of $\text{CaAl}_2\text{O}_4:\text{Eu}^{2+},\text{Nd}^{3+}$.¹⁵⁵

4.1.2 $\text{Sr}_4\text{Al}_4\text{O}_{25}:\text{Eu}^{2+},\text{Nd}^{3+}$

After combined with TiO_2 , $\text{Sr}_4\text{Al}_4\text{O}_{25}:\text{Eu}^{2+},\text{Nd}^{3+}$ can absorb and store light, which will supply light for the TiO_2 to remain photocatalytic reaction in the darkness.¹⁵⁶ Recently, Ag_3PO_4 was reported to show the absorption up to 600 nm, which might be activated by the phosphorescence with the wavelength of 490 nm emitting from $\text{Sr}_4\text{Al}_4\text{O}_{25}:\text{Eu}^{2+},\text{Nd}^{3+}$. Therefore, the introduction of Ag_3PO_4 into $\text{Sr}_4\text{Al}_4\text{O}_{25}:\text{Eu}^{2+},\text{Nd}^{3+}$ to form hybrid also could harvest persistent phosphorescence to degrade the pollutant after turning off the lamp irradiation.¹⁵⁷ Li et al.¹⁵⁷ prepared the $\text{Ag}_3\text{PO}_4/\text{Sr}_4\text{Al}_4\text{O}_{25}:\text{Eu}^{2+},\text{Nd}^{3+}$ composites by a simple

precipitation process, followed by mixing with a desired amount of $\text{Sr}_4\text{Al}_4\text{O}_{25}:\text{Eu}^{2+},\text{Nd}^{3+}$. The composite with 50 wt.% $\text{Sr}_4\text{Al}_4\text{O}_{25}:\text{Eu}^{2+},\text{Nd}^{3+}$ showed the highest photocatalytic activity with degradation rate of 100% in the dark at 10.5 h.¹⁵⁷

4.2 Zirconate phosphors

Intense violet blue long-lasting phosphorescence covering a wavelength range of 320-550 nm was observed from $\text{BaZrO}_3:\text{Mg}^{2+}$, which partially overlaps the absorption of the TiO_2 .¹⁵⁸ Therefore, the $\text{BaZrO}_3:\text{Mg}^{2+}$ may assist the photocatalytic activity of TiO_2 with mix phase of anatase and rutile at night. Ma et al.¹⁵⁸ synthesized $\text{BaZrO}_3:\text{Mg}^{2+}/\text{TiO}_2$ composites with the perovskite structure via solid-state reaction and sol-gel method. The photocatalytic activity of $\text{BaZrO}_3:\text{Mg}^{2+}/\text{TiO}_2$ composite (75 mg) was evaluated through the decomposition of MB (75 ml, 10 mg/l). Results revealed that the $\text{BaZrO}_3:\text{Mg}^{2+}$ supported the photocatalytic activity of TiO_2 under UV light irradiation (~90%) or in darkness after UV irradiation (10%).¹⁵⁸

Table 1 Photocatalytic activities of LCP/semiconductors composite photocatalysts

Photocatalysts	Phosphor types	Photocatalytic experiments parameters	Photocatalytic activity	Reference photocatalyst; Photocatalytic activity	Enhancement factor	Reference
$\text{Y}_3\text{Al}_5\text{O}_{12}:\text{Er}^{3+}/\text{Bi}_2\text{WO}_6$	UCP	phenol; solar light	51%; at 120 min	Bi_2WO_6 ; 32%	1.59	85
$\text{Y}_3\text{Al}_5\text{O}_{12}:\text{Er}^{3+}/\text{TiO}_2$	UCP	congo red; visible light	0.4767 h^{-1}	TiO_2 ; 0.0869 h^{-1}	5.49	73
$\text{Y}_3\text{Al}_5\text{O}_{12}:\text{Er}^{3+}/\text{TiO}_2$	UCP	acid red; sunlight	90 % at 60 min	TiO_2 ; 67%	1.34	89
$\text{Y}_3\text{Al}_5\text{O}_{12}:\text{Er}^{3+}/\text{TiO}_2/\text{ZrO}_2$	UCP	Azo Fuch sine; sunlight	90 % at 60 min	TiO_2 ; 28%	3.21	72
$\text{Yb}_{0.3}\text{Y}_{2.7}\text{Al}_5\text{N}_{0.01}\text{F}_{0.01}\text{O}_{11.98}:\text{Er}^{3+}/\text{TiO}_2$	UCP	acid red B dye; sunlight	92 %; at 60 min	-	-	90
$\text{YAlO}_3:\text{Er}^{3+}/\text{ZnO}$	UCP	acid red B; sunlight	86% ; at 60 min	ZnO ; 69%	1.25	98
$\text{YFeO}_3:\text{Er}^{3+}/\text{TiO}_2/\text{SAC}$	UCP	MO; visible light	92%; at 80 min	-	-	76
$\text{YF}_3:\text{Yb}^{3+},\text{Tm}^{3+}/\text{P25}/\text{graphene}$	UCP	MO; sunlight	78%; at 60 min	P25; 27%	2.89	102
$\text{YF}_3:\text{Yb}^{3+},\text{Tm}^{3+}/\text{TiO}_2$	UCP	MB; NIR light	58%; at 9 h	TiO_2 ; 0%	-	107
$\text{NaYF}_4:\text{Yb}^{3+},\text{Tm}^{3+}/\text{TiO}_2$	UCP	MB; NIR light	90%; at 12 h	-	-	119
$\text{CaF}_2:\text{Er}^{3+},\text{Tm}^{3+},\text{Yb}^{3+}/\text{BiVO}_4$	UCP	MO; NIR light	$0.11 \times 10^{-1} \text{ h}^{-1}$	-	-	83
$\text{CaF}_2,\text{Tm}^{3+},\text{Yb}^{3+}/\text{TiO}_2$	UCP	MO; NIR light	$2.67 \times 10^{-2} \text{ mg/lh}$	TiO_2 ; $2.19 \times 10^{-3} \text{ mg/lh}$	12.2	86
$10\text{BaF}_2:\text{NaF},\text{Na}_3\text{AlF}_6/\text{TiO}_2$	UCP	Reduction of CO_2 with H_2O ; visible light	179 $\mu\text{mol/g-cat}$	TiO_2 ; 0 $\mu\text{mol/g-cat}$	-	122
$\text{ZnO}/\text{Y}_3\text{Al}_5\text{O}_{12}:\text{Ce}^{3+}$	DCP	MB; visible light	93%; at 240 min	ZnO ; 13%	7.15	138
$\text{ZnO}/\text{Y}_2\text{O}_2\text{S}:\text{Eu}^{3+}$	DCP	MB; visible light	95%; at 240 min	ZnO ; 13%	7.31	126
$\text{ZnO}/\text{NaSrBO}_3:\text{Tb}^{3+}$	DCP	MB; visible light	97%; at 240 min	ZnO ; 13%	7.46	74

5. Summary and outlook

Semiconductor photocatalysis has become more prominent owing to its advantages of the use of vast additive chemicals or disinfectants and its mineralization aspects. The major challenges in photocatalysis are the limited light absorption in the incident solar spectrum and quick recombination of photo-generated charge carriers. Increasing the energy harvesting efficiency for endless solar energy under ambient conditions will continue to be one of the most important objectives in designing photocatalysts. In this review, our aim is to reveal the advances of LCP materials as spectral converters for enhancing the photocatalytic activity. The LCP/semiconductor composites display excellent photocatalytic activity compared to the traditional visible light driven photocatalysts. The incorporation of the LCP as spectral converters including UCP, DCP and LAP into semiconductors to form hybrid photocatalysts has proved to a promising method to enhance the solar energy harvesting ability and visible light photocatalytic activity. The UCP doped in the semiconductor can absorb the NIR or visible lights and then emit UV or visible lights, which can effectively excite the semiconductor to generate more electron-hole pairs and high active cavities, leading to the enhancement of photocatalytic activity of pure semiconductor due to the UC effect.^{76,80-82} The introduction of DCP in the wide band semiconductor by utilizing the light DC characteristics can absorb the high energy photon and emit the low energy photon at a longer wavelength, which can effectively excite the dye to generate more electron-hole pairs, and facilitate the self-sensitized degradation of MB, thus enhance the photocatalytic activity of wide band semiconductor. Such a light-converting ability of phosphors is promising to fulfil a simple and effective removal of dyes by adjusting the light emission of the phosphors to improve the self-sensitized degradation of dyes. Moreover, the increase of dye adsorption and visible light absorption as well as the reduction of electron-hole pair recombination should also be responsible for the enhancement of the photocatalytic performance for LCP/semiconductors hybrid materials compared to pure semiconductors. The semiconductor coupled with an appropriate amount of LAP could continuously degrade organic contaminants even after turning off the lamp irradiation owing to the long afterglow characteristics. However, from the point of view of industrialization and commercialization, many challenges remain in the areas of photocatalysis. The major drawback associated with the low quantum efficiency of LCP materials limits the practical application in photocatalysis. Investigations have been made to improve the quantum efficiency by using plasmatic resonance, photonic crystals, impurity doping, quantum dots sensitizers, and core-shell structure.¹⁵⁹ Furthermore, high power laser is really needed for some UCP to obtain the up-conversion characteristics, which decreased the photocatalytic activity and limit the practical application in the solar light photocatalysis. In addition, it is well known fact that energy transfer from semiconductor to lanthanide ions is common. Therefore, there is very high possibility of energy transfer back to lanthanide ions, even after absorbing the UC emission from lanthanide ions, which is not beneficial to the photocatalytic activity of LCP/semiconductors composites. Despite the encouraging progress to date, the application of LCP materials as spectral converters for photocatalysis is still at the primary stages.

The deepening knowledge of the photocatalytic mechanism and exploration of high quantum efficiency LCP/semiconductor composites are indispensable to make substantial breakthrough for practical applications.

Acknowledgement

Financial support from the National Natural Science Foundation of China (No. 21401180) is gratefully acknowledged.

Notes and references

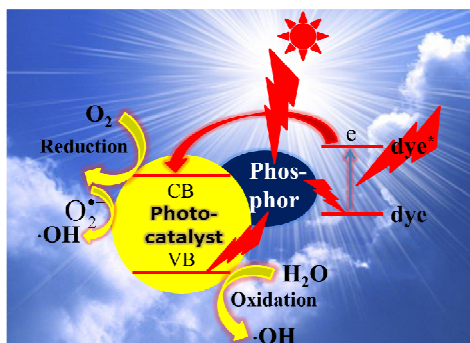
- ^aInstitute of Coordination Bond Metrology and Engineering, College of Materials Science and Engineering, China Jiliang University, Hangzhou 310018, China, Fax: +86 571 86872475; Tel: +86 571 86872475; E-mail address: lxj669635@126.com
- ^bEngineering Research Center for Nanophotonics & Advanced Instrument, Ministry of Education, Department of Physics, East China Normal University, Shanghai 200062, China, Fax: +86 21 62234321; Tel: +86 21 62234132; E-mail: lkpan@phy.ecnu.edu.cn
- 1 A. Fujishima and K. Honda, *Nature*, 1972, **238**, 37.
 - 2 J. H. Yang, D. Wang, H. X. Han and C. Li, *Acc. Chem. Res.*, 2013, **46**, 1900.
 - 3 X. B. Chen, S. H. Shen, L. J. Guo and S. S. Mao, *Chem. Rev.*, 2010, **110**, 6503.
 - 4 C. C. Chen, W. H. Ma and J. C. Zhao, *Chem. Soc. Rev.*, 2010, **39**, 4206.
 - 5 Q. J. Xiang, J. G. Yu and M. Jaroniec, *Chem. Soc. Rev.*, 2012, **41**, 782.
 - 6 X. J. Liu, L. K. Pan, T. Lv and Z. Sun, *J. Alloy. Compd.*, 2014, **583**, 390.
 - 7 X. J. Liu, L. K. Pan, T. Lv, G. Zhu, Z. Sun and C. Q. Sun, *Chem. Commun.*, 2011, **47**, 11984.
 - 8 J. L. Li, X. J. Liu, L. K. Pan, W. Qin, T. Q. Chen and Z. Sun, *RSC Adv.*, 2014, **4**, 9647.
 - 9 W. Q. Fan, Q. H. Zhang and Y. Wang, *Phys. Chem. Chem. Phys.*, 2013, **15**, 2632.
 - 10 N. Zhang, Y. H. Zhang and Y. J. Xu, *Nanoscale*, 2012, **4**, 5792.
 - 11 W. Wu, J. Changzhong and V. A. L. Roy, *Nanoscale*, 2015, **7**, 38.
 - 12 Z. W. Zhao, Y. J. Sun and F. Dong, *Nanoscale*, 2015, **7**, 15.
 - 13 Y. J. Wang, Q. S. Wang, X. Y. Zhan, F. M. Wang, M. Saifdar and J. He, *Nanoscale*, 2013, **5**, 8326.
 - 14 X. J. Liu, L. K. Pan, T. Q. Chen, J. L. Li, K. Yu, Z. Sun and C. Q. Sun, *Catal. Sci. Technol.*, 2013, **3**, 1805.
 - 15 R. Long and N. J. English, *Appl. Phys. Lett.*, 2011, **98**, 142103.
 - 16 T. Y. Zhao, Z. Y. Liu, K. Nakata, S. Nishimoto, T. Murakami, Y. Zhao, L. Jiang and A. Fujishima, *J. Mater. Chem.*, 2010, **20**, 5095.
 - 17 Y. F. Zhu, R. G. Du, W. Chen, H. Q. Qi and C. J. Lin, *Electrochem. Commun.*, 2010, **12**, 1626.
 - 18 H. Q. Tan, Z. Zhao, M. Niu, C. Y. Mao, D. P. Cao, D. J. Cheng, P. Y. Feng and Z. C. Sun, *Nanoscale*, 2014, **6**, 10216.
 - 19 Q. J. Xiang, J. G. Yu and M. Jaroniec, *Nanoscale*, 2011, **3**, 3670.
 - 20 M. R. Hoffmann, S. T. Martin, W. Choi and D. W. Bahnemann, *Chem. Rev.*, 1995, **95**, 69.
 - 21 L. Shi, L. Liang, J. Ma, F. X. Wang and J. M. Sun, *Catal. Sci. Technol.*, 2014, **4**, 758.
 - 22 A. S. Weber, A. M. Grady and R. T. Koodali, *Catal. Sci. Technol.*, 2012, **2**, 683.
 - 23 S. D. Sun, X. P. Song, Y. X. Sun, D. C. Deng and Z. M. Yang, *Catal. Sci. Technol.*, 2012, **2**, 925.

- 24 A. Ye, W. Q. Fan, Q. H. Zhang, W. P. Deng and Y. Wang, *Catal. Sci. Technol.*, 2012, **2**, 969.
- 25 Z. K. Zheng, B. B. Huang, X. D. Meng, J. P. Wang, S. Y. Wang, Z. Z. Lou, Z. Y. Wang, X. Y. Qin, X. Y. Zhang and Y. Dai, *Chem. Commun.*, 2013, **49**, 868.
- 26 R. Asahi, T. Morikawa, T. Ohwaki, K. Aoki and Y. Taga, *Science*, 2001, **293**, 269.
- 27 A. Pandikumar, S. Murugesan and R. Ramaraj, *ACS Appl. Mater. Interfaces*, 2010, **2**, 1912.
- 28 J. Bai, J. Li, Y. Liu, B. Zhou and W. Cai, *Appl. Catal. B: Environ.*, 2010, **95**, 408.
- 29 T. Ochiai, K. Nakata, T. Murakami, A. Fujishima, Y. Yao, D. A. Tryk and Y. Kubota, *Water Res.*, 2010, **44**, 904.
- 30 K. Lalitha, G. Sadanandam, V. D. Kumari, M. Subrahmanyam, B. Sreedhar and N. Y. Hebalkar, *J. Phys. Chem. C*, 2010, **114**, 22181.
- 31 Q. Li, T. Kako and J. Ye, *J. Mater. Chem.*, 2010, **20**, 10187.
- 32 P. S. S. Kumar, M. R. Raj, S. Anandan, M. F. Zhou and M. Ashokkumar, *Water Sci. Technol.*, 2009, **60**, 1589.
- 33 J. J. Wu and C. H. Tseng, *Appl. Catal. B: Environ.*, 2006, **66**, 51.
- 34 Y. Ma, J. W. Fu, X. Tao, X. Li and J. F. Chen, *Appl. Surf. Sci.*, 2011, **257**, 5046.
- 35 W. Zhang, L. D. Zou and L. Z. Wang, *Chem. Eng. J.*, 2011, **168**, 485.
- 36 B. Naik, K. M. Parida and C. S. Gopinath, *J. Phys. Chem. C*, 2010, **114**, 19473.
- 37 D. Lin, H. Wu, R. Zhang and W. Pan, *Chem. Mater.*, 2009, **21**, 3479.
- 38 X. J. Liu, L. K. Pan, T. Lv, G. Zhu, T. Lu, Z. Sun and C. Q. Sun, *RSC Adv.*, 2011, **1**, 1245.
- 39 X. J. Liu, L. K. Pan, T. Lv, T. Lu, G. Zhu, Z. Sun and C. Q. Sun, *Catal. Sci. Technol.*, 2011, **1**, 1189.
- 40 W. Yu, X. J. Liu, L. K. Pan, J. L. Li, J. Y. Liu, J. Zhang, P. Li, C. Chen and Z. Sun, *Appl. Surf. Sci.*, 2014, **319**, 107.
- 41 Q. J. Xiang, J. G. Yu and M. Jaroniec, *Phys. Chem. Chem. Phys.*, 2011, **13**, 4853.
- 42 X. J. Liu, L. K. Pan, T. Lv, Z. Sun and C. Q. Sun, *RSC Adv.*, 2012, **2**, 3823.
- 43 C. H. An, J. Z. Wang, W. Jiang, M. Y. Zhang, X. J. Ming, S. T. Wang and Q. H. Zhang, *Nanoscale*, 2012, **4**, 5646.
- 44 Y. Li, H. Zhang, Z. Guo, J. Han, X. Zhao, Q. Zhao and S. J. Kim, *Langmuir*, 2008, **24**, 8351.
- 45 C. H. An, S. Peng and Y. G. Sun, *Adv. Mater.*, 2010, **22**, 2570.
- 46 L. Zhao, X. F. Chen, X. C. Wang, Y. J. Zhang, W. Wei, Y. H. Sun, M. Antonietti and M. M. Titirici, *Adv. Mater.*, 2010, **22**, 3317.
- 47 M. Wu, J. M. Yan, X. N. Tang, M. Zhao and Q. Jiang, *ChemSusChem*, 2014, **7**, 2654.
- 48 Z. H. Xu and J. G. Yu, *Nanoscale*, 2011, **3**, 3138.
- 49 J. Jiang and L. Zhang, *Chem. Eur. J.*, 2011, **17**, 3710.
- 50 X. F. Wang, S. F. Li, H. G. Yu, J. G. Yu and S. W. Liu, *Chem. Eur. J.*, 2011, **17**, 7777.
- 51 G. H. Jiang, R. J. Wang, X. H. Wang, X. G. Xi, R. B. Hu, Y. Zhou, S. Wang, T. Wang and W. X. Chen, *ACS Appl. Mater. Interfaces*, 2012, **4**, 4440.
- 52 S. B. Zhu, T. G. Xu, H. B. Fu, J. C. Zhao and Y. F. Zhu, *Environ. Sci. Technol.*, 2007, **41**, 6234.
- 53 J. X. Low, J. G. Yu, Q. Li and B. Cheng, *Phys. Chem. Chem. Phys.*, 2014, **16**, 1111.
- 54 Z. Sun, J. Guo, S. Zhu, L. Mao, J. Ma and D. Zhang, *Nanoscale*, 2014, **6**, 2186.
- 55 D. H. Wang, G. Q. Gao, Y. W. Zhang, L. S. Zhou, A. W. Xu and W. Chen, *Nanoscale*, 2012, **2**, 7780.
- 56 H. F. Cheng, B. B. Huang and Y. Dai, *Nanoscale*, 2014, **6**, 2009.
- 57 L. Z. Zhang, I. Djerdj, M. Cao, M. Antonietti and M. Niederberger, *Adv. Mater.*, 2007, **19**, 2083.
- 58 F. Y. Shen, W. X. Que, Y. L. Liao and X. T. Yin, *Ind. Eng. Chem. Res.*, 2011, **50**, 9131.
- 59 T. Matoba, K. Maeda and K. Domen, *Chem. Eur. J.*, 2011, **17**, 14731.
- 60 J. Y. Shi, G. J. Liu, N. Wang and C. Li, *J. Mater. Chem.*, 2012, **22**, 18808.
- 61 M. S. Gui and W. D. Zhang, *J. Phys. Chem. Solids*, 2012, **73**, 1342.
- 62 Y. S. Fu, X. Q. Sun and X. Wang, *Mater. Chem. Phys.*, 2011, **131**, 325.
- 63 Y. L. Min, K. Zhang, Y. C. Chen and Y. G. Zhang, *Sep. Purif. Technol.*, 2012, **86**, 98.
- 64 D. James and T. Zubkov, *J. Photochem. Photobiol. A: Chem.*, 2013, **262**, 45.
- 65 S. Liu, J. Q. Tian, L. Wang, Y. L. Luo and X. P. Sun, *Catal. Sci. Technol.*, 2012, **2**, 339.
- 66 C. Hu, T. W. Peng, X. X. Hu, Y. L. Nie, X. F. Zhou, J. H. Qu and H. He, *J. Am. Chem. Soc.*, 2009, **132**, 857.
- 67 S. F. Chen, W. Zhao, W. Liu, H. Y. Zhang, X. L. Yu and Y. H. Chen, *J. Hazard. Mater.*, 2009, **172**, 1415.
- 68 X. F. Zhou, C. Hu, X. X. Hu, T. W. Peng and J. H. Qu, *J. Phys. Chem. C*, 2010, **114**, 2746.
- 69 J. J. Fan, L. Zhao, J. G. Yu and G. Liu, *Nanoscale*, 2012, **4**, 6597.
- 70 G. Zhu, X. J. Wang, H. L. Li, L. K. Pan, H. C. Sun, X. J. Liu, T. Lv and Z. Sun, *Chem. Commun.*, 2012, **48**, 958.
- 71 X. J. Wang, M. C. Zhang, H. Ding, H. L. Li and Z. Sun, *J. Alloys Compd.*, 2011, **509**, 6317.
- 72 L. N. Yin, J. Q. Gao, J. Wang, X. Y. Luan, P. L. Kang, Y. Li, K. Li and X. D. Zhang, *Res. Chem. Intermed.*, 2012, **38**, 523.
- 73 J. Wang, R. H. Li, Z. H. Zhang, W. Sun, R. Xu, Y. P. Xie, Z. Q. Xing and X. D. Zhang, *Appl. Catal. A: Gen.*, 2008, **334**, 227.
- 74 X. J. Liu, X. J. Wang, H. L. Li, J. L. Li, L. K. Pan, J. Zhang, G. Q. Min, Z. Sun and C. Q. Sun, *Dalton Trans.*, 2015, **44**, 97.
- 75 C. H. Li, F. Wang, J. Zhu and J. C. Yu, *Appl. Catal. B: Environ.*, 2010, **100**, 433.
- 76 D. X. Hou, L. Feng, J. B. Zhang, S. S. Dong, D. D. Zhou and T. T. Lim, *J. Hazard. Mater.*, 2012, **199-200**, 301.
- 77 G. J. Feng, S. W. Liu, Z. L. Xiu, Y. Zhang, J. X. Yu, Y. Chen, P. Wang and X. J. Yu, *J. Phys. Chem. C*, 2008, **112**, 13692.
- 78 Z. J. Zhang, W. Z. Wang, W. Z. Yin, M. Shang, L. Wang and S. M. Sun, *Appl. Catal. B: Environ.*, 2010, **101**, 68.
- 79 H. Tong, S. X. Ouyang, Y. P. Bi, N. Umezawa, M. Oshikiri and J. H. Ye, *Adv. Mater.*, 2012, **24**, 229.
- 80 Y. N. Tang, W. H. Di, X. S. Zhai, R. Y. Yang and W. P. Qin, *ACS Catal.*, 2013, **3**, 405.
- 81 C. C. Wang, K. L. Song, Y. Feng, D. G. Yin, J. Ouyang, B. Liu, X. Z. Cao, L. Zhang, Y. L. Han and M. H. Wu, *RSC Adv.*, 2014, **4**, 39118.
- 82 D. X. Xu, Z. W. Lian, M. L. Fu, B. L. Yuan, J. W. Shi and H. J. Cui, *Appl. Catal. B: Environ.*, 2013, **142-143**, 377.
- 83 S. Q. Huang, Z. Y. Lou, N. W. Zhu, L. Gu, C. Miao, H. P. Yuan and A. Shan, *Nanoscale*, 2014, 1362.

- 84 S. Q. Huang, Z. Y. Lou, A. D. Shan, N. W. Zhu, K. L. Feng and H. P. Yuan, *J. Mater. Chem. A*, 2014, **2**, 16165.
- 85 Z. J. Zhang, W. Z. Wang, J. Xu, M. Shang, J. Ren and S. M. Sun, *Catal. Commun.*, 2011, **13**, 31.
- 86 S. Q. Huang, L. Gu, C. Miao, Z. Y. Lou, N. W. Zhu, H. P. Yuan and A. D. Shan, *J. Mater. Chem. A*, 2013, **1**, 7874.
- 87 T. G. Li, S. W. Liu, H. P. Zhang, E. H. Wang, L. J. Song and P. Wang, *J. Mater. Sci.*, 2011, **46**, 2882.
- 88 W. Tobler and W. Durisch, *Appl. Energy*, 2008, **85**, 483.
- 89 J. Wang, Y. Xie, Z. Zhang, J. Li, Z. Jiang, Z. Xing, R. Xu and X. Zhang, *Russ. J. Phys. Chem. A*, 2009, **83**, 2350.
- 90 L. Yin, Y. Li, J. Wang, Y. Zhai, J. Wang, B. Wang, G. Han and P. Fan, *J. Mol. Catal. A: Chem.*, 2012, **363–364**, 265.
- 91 J. Wang, J. Li, B. Liu, Y. P. Xie, G. X. Han, Y. Li, L. Q. Zhang and X. D. Zhang, *Water Sci. Technol.*, 2009, **60**, 917.
- 92 H. G. Yang, Z. W. Dai and Z. W. Sun, *J. Lumin.*, 2007, **124**, 207.
- 93 J. Wang, J. Li, Y. F. Xie, C. W. Li, G. X. Han, L. Q. Zhang, R. Xu and X. D. Zhang, *J. Environ. Manage.*, 2010, **91**, 677.
- 94 J. Q. Gao, X. Y. Luan, J. Wang, B. X. Wang, K. Li, Y. Li, P. L. Kang and G. X. Han, *Desalination*, 2011, **268**, 68.
- 95 R. Xu, J. Li, J. Wang, X. F. Wang, B. Liu, B. X. Wang, X. Y. Luan and X. D. Zhang, *Sol. Energy Mater. Sol. Cells*, 2010, **94**, 1157.
- 96 J. Wang, J. Li, L. Zhang, C. Li, Y. Xie, B. Liu, R. Xu and X. Zhang, *Catal. Lett.*, 2009, **130**, 551.
- 97 J. Wang, Y. P. Xie, Z. H. Zhang, J. Li, C. W. Li, L. Q. Zhang, Z. Q. Xing, R. Xu and X. D. Zhang, *Environ. Chem. Lett.*, 2010, **8**, 87.
- 98 J. Wang, Y. P. Xie, Z. H. Zhang, J. Li, X. Chen, L. Q. Zhang, R. Xu and X. D. Zhang, *Sol. Energy Mater. Sol. Cells*, 2009, **93**, 355.
- 99 J. Wang, J. Li, Y. F. Xie, L. Q. Zhang, G. X. Han, Y. Li, R. Xu and X. D. Zhang, *Inorg. Mater.*, 2010, **46**, 399.
- 100 S. S. Dong, J. B. Zhang, L. L. Gao, Y. L. Wang and D. D. Zhou, *Trans. Nonferrous Met. Soc. China*, 2012, **22**, 2477.
- 101 A. Ivaturi, S. K. W. MacDougall, R. Martin-Rodriguez, M. Quintanilla, J. Marques-Hueso, K. W. Kramer, A. Meijerink and B. S. Richards, *J. Appl. Phys.*, 2013, **114**,
- 102 L. Ren, X. Qi, Y. D. Liu, Z. Y. Huang, X. L. Wei, J. Li, L. W. Yang and J. X. Zhong, *J. Mater. Chem.*, 2012, **22**, 11765.
- 103 H. h. Li and Y. h. Wang, *Res. Chem. Intermed.*, 2010, **36**, 51.
- 104 J. J. Guo, S. M. Zhu, Z. X. Chen, Y. Li, Z. Y. Yu, Q. L. Liu, J. B. Li, C. L. Feng and D. Zhang, *Ultrason. Sonochem.*, 2011, **18**, 1082.
- 105 R. J. Dillon, J. B. Joo, F. Zaera, Y. Yin and C. J. Bardeen, *Phys. Chem. Chem. Phys.*, 2013, **15**, 1488.
- 106 N. Zhang, S. Liu and Y. J. Xu, *Nanoscale*, 2012, **4**, 2227.
- 107 W. P. Qin, D. S. Zhang, D. Zhao, L. L. Wang and K. Z. Zheng, *Chem. Commun.*, 2010, **46**, 2304.
- 108 Q. L. Ye, X. Yang, C. Li and Z. Li, *Mater. Lett.*, 2013, **106**, 238.
- 109 J. de Wild, J. K. Rath, A. Meijerink, W. G. J. H. M. van Sark and R. E. I. Schropp, *Sol. Energy Mater. Sol. Cells*, 2010, **94**, 2395.
- 110 J. C. Boyer and F. C. J. M. van Veggel, *Nanoscale*, 2010, **2**, 1417.
- 111 W. Huang, W. J. Huang, Y. Ni, C. H. Lu, L. J. Tan and Z. Z. Xu, *Appl. Surf. Sci.*, 2013, **282**, 832.
- 112 Y. X. Ye, X. Y. Hu, Z. Y. Yan, E. Z. Liu, J. Fan, D. K. Zhang, H. Miao, Y. B. Shang and J. Yang, *Chin. Phys. B*, 2011, **20**, 087803.
- 113 S. Heer, K. Kompe, H. U. Gudel and M. Haase, *Adv. Mater.*, 2004, **16**, 2102.
- 114 S. J. Budijono, J. Shan, N. Yao, Y. Miura, T. Hoye, R. H. Austin, Y. Ju and R. K. Prud'homme, *Chem. Mater.*, 2009, **22**, 311.
- 115 X. Y. Guo, W. H. Di, C. F. Chen, C. X. Liu, X. Wang and W. P. Qin, *Dalton Trans.*, 2014, **43**, 1048.
- 116 X. Y. Wu, S. Yin, Q. Dong, B. Liu, Y. H. Wang, T. Sekino, S. W. Lee and T. Sato, *Sci. Rep.*, 2013, **3**, 2918.
- 117 W. Wang, M. Y. Ding, C. H. Lu, Y. Ni and Z. Z. Xu, *Appl. Catal. B: Environ.*, 2014, **144**, 379.
- 118 X. Y. Guo, W. Y. Song, C. F. Chen, W. H. Di and W. P. Qin, *Phys. Chem. Chem. Phys.*, 2013, **15**, 14681.
- 119 Y. W. Zhang and Z. L. Hong, *Nanoscale*, 2013, **5**, 8930.
- 120 W. Wang, W. J. Huang, Y. Ni, C. H. Lu and Z. Z. Xu, *ACS Appl. Mater. Interfaces*, 2014, **6**, 340.
- 121 G. F. Wang, Q. Peng and Y. D. Li, *J. Am. Chem. Soc.*, 2009, **131**, 14200.
- 122 E. Z. Liu, J. Fan, X. Y. Hu, W. Q. Hou and H. Z. Dai, *Chin. Phys. B*, 2012, **21**, 043403.
- 123 J. Wang, G. Zhang, Z. H. Zhang, X. D. Zhang, G. Zhao, F. Y. Wen, Z. J. Pan, Y. Li, P. Zhang and P. L. Kang, *Water Res.*, 2006, **40**, 2143.
- 124 J. Wang, T. Ma, G. Zhang, Z. H. Zhang, X. D. Zhang, Y. F. Jiang, G. Zhao and P. Zhang, *Catal. Commun.*, 2007, **8**, 607.
- 125 J. Wang, F. Y. Wen, Z. H. Zhang, X. D. Zhang, Z. J. Pan, P. Zhang, P. L. Kang, J. Tong, L. Wang and L. Xu, *J. Photochem. Photobiol. A: Chem.*, 2006, **180**, 189.
- 126 X. J. Liu, L. K. Pan, J. L. Li, K. Yu, Z. Sun and C. Q. Sun, *J. Colloid Interface Sci.*, 2013, **404**, 150.
- 127 Z. G. Xiong, L. L. Zhang, J. Z. Ma and X. S. Zhao, *Chem. Commun.*, 2010, **46**, 6099.
- 128 F. Han, V. S. R. Kambala, M. Srinivasan, D. Rajarathnam and R. Naidu, *Appl. Catal. B: Environ.*, 2009, **359**, 25.
- 129 P. F. Ji, J. L. Zhang, F. Chen and M. Anpo, *Appl. Catal. B: Environ.*, 2009, **85**, 148.
- 130 L. Pan, J. J. Zou, X. Y. Liu, X. J. Liu, S. b. Wang, X. W. Zhang and L. Wang, *Ind. Eng. Chem. Res.*, 2012, **51**, 12782.
- 131 Y. Yan, H. P. Sun, P. P. Yao, S. Z. Kang and J. Mu, *Appl. Surf. Sci.*, 2011, **257**, 3620.
- 132 T. Lv, L. K. Pan, X. J. Liu, T. Lu, G. Zhu, Z. Sun and C. Q. Sun, *Catal. Sci. Technol.*, 2012, **2**, 754.
- 133 B. O'Regan and M. Grätzel, *Nature*, 1991, **353**, 737.
- 134 S. Cho, J. W. Jang, S. Hwang, J. S. Lee and S. H. Kim, *Langmuir*, 2012, **28**, 17530.
- 135 H. C. Sun, L. K. Pan, G. Zhu, X. Q. Piao, L. Zhang and Z. Sun, *Dalton Trans.*, 2014, **43**, 14936.
- 136 J. Q. Liu, X. J. Wang, T. T. Xuan, H. L. Li and Z. Sun, *J. Alloys Compd.*, 2014, **593**, 128.
- 137 J. Q. Liu, X. J. Wang, T. T. Xuan, C. B. Wang, H. L. Li and Z. Sun, *J. Lumin.*, 2015, **158**, 322.
- 138 X. J. Liu, X. J. Wang, H. L. Li, L. K. Pan, T. Lv, Z. Sun and C. Q. Sun, *J. Mater. Chem.*, 2012, **22**, 16293.
- 139 X. D. Jiang, Y. Q. Wang and C. X. Pan, *J. Alloys Compd.*, 2011, **509**, L137.
- 140 J. B. Zhong, J. L. Wang, L. Tao, M. C. Gong, L. Zhimin and Y. Q. Chen, *J. Hazard. Mater.*, 2007, **139**, 323.
- 141 Bum Goo Kim, Hak Guen Lee, Hee Sung Kim and Y. S. Kim, *Bull. Korean Chem. Soc.*, 2009, **30**, 675.

- 142 Y. Zheng, J. Lin and Q. Wang, *Photochem. Photobiol. Sci.*, 2012, **11**, 1567.
- 143 H. N. Luitel, R. Chand, T. Torikai, M. Yada and T. Watari, *Int. J. Photoenergy*, 2013, **2013**, Article ID 410613.
- 5 144 H. Sun, L. Pan, X. Piao and Z. Sun, *J. Colloid Interface Sci.*, 2014, **416**, 81.
- 145 S. Li, W. C. Wang, Y. Q. Chen, L. J. Zhang, J. X. Guo and M. C. Gong, *Catal. Commun.*, 2009, **10**, 1048.
- 146 J. H. Yoon and J. S. Kim, *Ionics*, 2010, **16**, 131.
- 10 147 J. H. Yoon, S. C. Jung and J. S. Kim, *Mater. Chem. Phys.*, 2011, **125**, 342.
- 148 H. Li, S. Yin, Y. Wang and T. Sato, *J. Catal.*, 2012, **286**, 273.
- 149 H. H. Li, S. Yin and T. Sato, *Appl. Catal. B: Environ.*, 2011, **106**, 586.
- 15 150 H. H. Li, S. Yin and T. Sato, *Nanoscale Res. Lett.*, 2011, **6**, 5.
- 151 H. H. Li, S. Yin, Y. H. Wang and T. Sato, *J. Mol. Catal. A: Chem.*, 2012, **363**, 129.
- 152 H. H. Li, S. Yin, Y. H. Wang and T. Sato, *Environ. Sci. Technol.*, 2012, **46**, 7741.
- 20 153 H. Li, S. Yin, Y. Wang and T. Sato, *RSC Adv.*, 2012, **2**, 3234.
- 154 H. Li, S. Yin, Y. Wang, T. Sekino, S. W. Lee and T. Sato, *J. Catal.*, 2012, **297**, 65.
- 155 H. Li, S. Yin, Y. Wang and T. Sato, *J. Am. Ceram. Soc.*, 2013, **96**, 1258.
- 25 156 J. Zhang, F. Pan, W. Hao, Q. Ge and T. Wang, *Appl. Phys. Lett.*, 2004, **85**, 5778.
- 157 H. H. Li, S. Yin, Y. H. Wang, T. Sekino, S. W. Lee and T. Sato, *J. Mater. Chem. A*, 2013, **1**, 1123.
- 158 X. L. Ma, J. C. Zhang, H. H. Li, B. C. Duan, L. N. Guo, M. D. Que
30 and Y. H. Wang, *J. Alloys Compd.*, 2013, **580**, 564.
- 159 W. H. Zhang, F. Ding and S. Y. Chou, *Adv. Mater.*, 2012, **24**, OP236.

Graphical Contents Entry



Light-conversion phosphors-based composites including up-conversion, down-conversion, and long afterglow phosphors-semiconductor for efficient photocatalysis are summarized.